Communications on Applied Nonlinear Analysis
ISSN: 1074-133X
Vol 32 No. ICMASD (2025)

A Study on Wind Load Analysis of High Rise Building using CFD

Ranjeet Kumar Sahani[1], Vishwa Mohini Rai[1]

[1]Department of Civil Engineering, CT University, India

Corresponding Author's E-mail: Ranjeet.sahani976@gmail.com

Article History:

Received: 12-12-2024

Revised: 25-01-2025

Accepted: 05-02-2025

Abstract:

This research show the effects of external wind flow conditions on the high rise building's stability having balconies and without balconies as well. It focuses on how corner treatment techniques of balconies and buildings such as flow spoilers, chamfering, and tapering wind-induced forces reduce the effects of uplift, shear, and lateral loads on the high rise buildings. Computational Fluid Dynamics (CFD) simulations were conducted on structure for this research by using ANSYS software for CAD modelling to analyze wind pressure, velocity profiles, and lateral deformation. After that static structural analysis was performed to evaluate shear stress and deformation produced under wind loads, according to IS 875 Part III standards.

The study helps to reduce drag forces and improve structural integrity by the help of aerodynamic edge treatments without changing the structural parts of buildings. Providing chamfered and tapered designs of high rise building, the drag forces were reduced by up to 40% which helps to enhance the structural safety and performance. The flow spoilers and chamfering of corners in high rise structure reduce wind loads and optimize structural serviceability.

Integrating aerodynamic considerations into high-rise building designs, particularly in regions prone to severe wind conditions will solve the challenges which arise due to wind vibrations and deformation, and provide long-term resilience and safety to structure.

In conclusion, The research show attention to the practical implications of aerodynamic designs in modern structural engineering world by providing actionable insights into effective design strategies, wind-structure interaction and offering guidelines for architects and engineers. Using CFD helps to design advanced sustainable and efficient high-rise construction.

Keywords: Computational Fluid Dynamics (CFD) for Wind Load Analysis, Aerodynamic Corner Treatments in Balcony Design, Drag Coefficient in High-Rise Structures, Wind Tunnel Testing for Structural Aerodynamics, Pressure and Velocity Profiles in Building Structures, Chamfer and Fillet Modifications for Wind Force Mitigation.

1. Introduction

As per the NOAA data, the intensity of cyclones and wind gusts impacting low rise and high rise building structure has increased causing heavy damage and destruction. The damage cost and deaths has increased manifold in last 10 years. The hurricane "Katrina" has become the costliest in the

history which was “category 3” type hurricane and causing immense damage to building structures and more than 1900 deaths [23].

The external air flow conditions (wind fluctuations) causes damages to structure by making roof membranes flutter and flap due to uplift pressure [24,25]. The loss of roofing causes various problems like “rainwater intrusion, interior restoration and occupant displacement” [26]. The intermittent suction is generated by the corner vortices which are due to uplift pressure. The debris which is airborne causes damage to other structure when wind is in downward direction [27]. The primary cause of aerodynamic stresses on a low building's roof and walls is the interaction between wind flow and the building's surface. The behavior of this interaction is primarily determined by the geometry and flow characteristics of the building. However, it is common for architects and engineers to overlook these factors during the construction of buildings. Instead, they tend to prioritize the structural and design elements of the structure, such as walls, overhangs, foundations, and roofs.

The evaluation of building structure under external load conditions was previously conducted using wind tunnel testing. The experimental testing was based on determination of drag force and pressure coefficients. However, the recent techniques are based on usage of Computational Fluid Dynamics (CFD) for evaluation of structure stability. The CFD analysis requires data on type of external air flow, magnitude of air flow and turbulence conditions. The CFD technique aims to develop more reliable models which can better predict the damage caused due to high wind flow conditions and aid in developing more robust designs.

The use of Computational Fluid Dynamics (CFD) techniques is becoming more widely recognized as a reliable approach for predicting turbulent flow over structures and impacting their design. The reason for this is the possibility of experimental procedures being both time-consuming and costly. Computational fluid dynamics (CFD) methods not only simulate the flow field surrounding a building but also predict various parameters including temperature, pressure, and velocity fields. The methodologies discussed here are readily available and can be easily implemented in the field of design. Computational fluid dynamics (CFD) methodologies are being utilized by various industries.

1.2 CFD simulations for building design

The wind tunnel testing process was expensive and time consuming which were replaced by CFD in 1950’s. The fluid flow predictions are determined from CFD using computer simulation packages. The advent of digital computers technology made use of CFD technique popular and widespread. Computational Fluid Dynamics (CFD) analysis is currently employed in various fields, such as wind engineering, hydrology, oceanography, meteorology, nuclear power, marine engineering, electrical and electronic engineering, biomedical engineering, chemical engineering, and environmental engineering. The current understanding differs significantly from the previous notion that CFD analysis was only applicable to aerodynamic research [33]. The range and applicability of CFD increased widely and is now implemented in both architectural, engineering and HVAC designs. The market today has various types of CFD simulation packages. The use of CFD in pedestrian wind comfort is shown in figure 1.1 below.

In building structure, the CFD is used to investigate the external as well as internal environment affecting stability of structure and building envelope [34]. Computational Fluid Dynamics (CFD) is a method that can be utilized to analyze the effects of wind on various structures, including buildings, bridges, and street canyons. The primary objective is to predict and forecast the behavior of wind flows in outdoor settings. Comprehending the functioning of a Computational Fluid Dynamics (CFD) code for a particular application is of utmost importance to ensure the validity of the obtained results. Additionally, a strong understanding of fluid mechanics is necessary to critically evaluate the findings derived from CFD simulations [36]. However, the cost of commercial CFD package is very high.

1.3. General use of CFD as a design assistance tool

The American Institute of Architects (AIA) has provided a comprehensive overview of the complex nature of design and construction projects in their publication titled "The Five Phases of Design." The initial stage is the phase during which the most critical decisions are made. During the requirements phase, stakeholders engage in discussions pertaining to the project's requirements. They communicate their expectations to the design team, including factors such as the number of residents, functionalities, and the quantity of accommodations. The scope of the design endeavor is determined by the interactions that take place. Schematic drawings are typically generated after the initial phase of product definition. During the schematic design phase, the owner is provided with drawings, papers, or other materials that depict the design's principles and include elements like form, scale, and spatial linkages. The purpose of the proprietor is to assess and evaluate these materials. The design development phase is the third phase of the project. During this phase, architectural documents are provided which comprehensively describe the mechanical, electrical, hydraulic, and structural components of the project. The ideas generated in the second segment are expanded upon in subsequent stages. Construction documents are typically produced after the design development phase has been completed. The general contractor or builder is typically hired after the completion of the construction documentation, which follows the five phases of design outlined by the AIA. During the schematic stage, Computational Fluid Dynamics (CFD) is commonly utilized for the calculation and analysis of air movement within and around buildings. The evaluation process typically determines whether the design needs to be modified based on the calculated results. The building's interior and external environmental conditions will meet the specified standards through iterative repetition of the methods [41]. Computational fluid dynamics (CFD) techniques are commonly utilized as a design assistance tool, as mentioned earlier. CFD simulations can be advantageous for architects and designers during the conceptual design phase as they can improve the indoor and outdoor environments of a proposed structure. The application of computational fluid dynamics (CFD) simulation in the architectural design process is demonstrated in Figure 1.5. This study provides recommendations for ensuring the effective utilization of computational fluid dynamics (CFD) simulation results in the design of buildings. It also demonstrates how the CFD process can be used as a tool to aid in design decision-making [37].

1.4. Limitations of CFD tool

CFD solves a series of mathematical equations to examine the air velocity, temperature, pollutant concentrations, and degree of turbulence around a structure in order to anticipate the flow of air inside and around it. In order to determine the required computing inputs, mathematical modeling must be done beforehand. Contrary to other building simulations, including energy simulations, CFD requires some familiarity with numerical techniques and an understanding of mathematical modeling. Furthermore, the CFD modeling methodology depends on physical models like turbulence. However, boundary conditions are not always well-known and computational domains for studies of outside environments might be quite extensive [42].

1.5. Fluid Structure Interaction (FSI studies)

The multiphysics study of the interaction between fluids and structures is known as fluid-structure interaction, or FSI. The structure may be subjected to heat loads or pressure from the fluid flow. These loads might alter the structure in a way that modifies the fluid flow itself. As the degree of fluid-structure interaction grows, your product can experience more undesirable impacts. To guarantee the lifetime, dependability, and safety of your product, you may have a better knowledge of the phenomena that occur with it by using ANSYS simulation. For each fluid-structure interaction problem, ANSYS offers a variety of solutions that provide the required degree of realism. ANSYS CFD can tackle simple fluid-structure interaction issues in their entirety. An impeller revolving in a mixing tank is an example of rigid body motion. When the fluid-structure interaction grows and a more thorough analysis of the issue is required, ANSYS offers a simple, automated solution known as one-way coupling. A one-way coupling automatically transmits and translates the data to the other system while solving the original CFD or ANSYS Mechanical simulation. An example of this would be to automatically transfer the data obtained from modeling the fluid flow around a cone flow meter in order to compute the structural reaction that results.

2. Theoretical Framework/Theory/Literature Review

Hussein et al. [1] have conducted wind tunnel experiments on different types of low rise buildings for determination of mean pressure coefficients and surface flow fields. Different building type shapes and array of structures are investigated and best design shape is determined.

Hold et al. [2] have conducted numerical investigation on pitched roof building to determine the effect of power fluctuation on pressure/drag force generated on building. The numerical investigations are conducted for different wind angle of attack.

Richardson et. al. [3] have conducted experimental investigation on 4 small scaled pitched roof building to determine variation of pressure and drag force generated on the structure. The research findings have shown an increase in pressure generated on structure with increase in wind velocity.

Xu et. al [4] have conducted experimental investigation on building structure having hip shaped design using wind tunnel testing method. The variation of wind pressure with respect to “hip height” was investigated and drag coefficient values are determined for the same.

Ginger et al. [5] have conducted experimental investigation on building structure having low-rise pitched roof. The experimental investigation conducted on building structure is based on wind tunnel testing method. The variable investigated was “length to span” ratio on external air pressure conditions.

Guirguis et al. [6] have conducted experimental investigation on high rise building structure. The investigations were carried out using wind tunnel testing method. The output parameters generated are pressure distribution plot and temperature distribution plot on mono slope small scale model.

Ntinas et al. [7] have conducted numerical investigation on building structure having different shape structures and obstacles. The shape structure investigated is pitched roof type and arched shape. The pressure, velocity and turbulence kinetic energy is determined for different cases.

Sabransky et al. [8] have conducted numerical investigation on building structure subjected to different varying aerodynamic loads. The CAD design of building is structure is shown in figure 2.1 below and meshed model of structure is shown in figure 2.2 below.

Tominaga et al. [9] have conducted experimental investigation on gable building structure using wind tunnel. Three different types of Gable buildings are investigated having different roof pitches. The pressure variation and drag force are evaluated for different designs for circular silos with conical roofs.

Yasushi Uematsu et al. [10], tested a small-scale model of spherical domes with different rise/span and height/span ratios for two kinds of turbulent boundary layers.

Tavakol et al. [11] have conducted investigation on surface-mounted hemisphere structure using experimental techniques as well as numerical techniques. The height of surface-mounted hemisphere is kept fixed and 2 different boundary layers are also considered. The turbulent boundary layers taken for analysis are thick type and thin type.

Rizzo et. al. [12] has conducted experimental investigation on structure with “hyperbolic paraboloid roofs” having different shapes. The pressure coefficient is determined from the analysis and comparative studies are done to determine performance of circular shape geometry and elliptical shape geometry.

Gavanski et. al. [13] have conducted experimental investigation on house structure using wind tunnel experiments. The house material taken for the analysis was wooden type and roof sheathing effect was investigated. Different geometry types of house structure and nearby condition like upstream terrain, surrounding structure along roof shape and building height are also investigated.

Yang et al. [14] have conducted numerical investigation on steel transmission tower using techniques of Computational Fluid Dynamics. The drag coefficient and drag force obtained from CFD analysis are in close agreement with experimental testing results.

Tamura et al. [15] have conducted numerical investigation of flow across rectangular cylinder using CFD. The aerodynamic studies conducted enabled to investigate the aero elastic instability

from 3 dimensional flow.

Kindangen et al. [16] have conducted numerical investigation of low rise building using techniques of CFD. The CFD investigation was conducted from along 5 directions and the analysis was conducted for hip roofs, mono slope and double slopes.

Shklyar et al. [17] have conducted numerical investigation on full scale greenhouse using techniques of computational fluid dynamics. The 3D isothermal flow pattern was analyzed. The results obtained for single-span pitched roof are compared with experimental results conducted on full scale model.

Nakayama et al. [18] have conducted numerical investigation on complex truss using LES model which is large eddy scale model. The mean drag coefficient values are determined for dynamic fluctuation conditions and the results obtained are on close agreement with empirical values.

Ahmad et al. [19] have conducted numerical investigation of low rise structures using 2D CFD simulation model. The CFD investigation was conducted for flat roofs and pitched roof building. The pitch slopes considered for the analysis was 10°, 20°& 30^0. The numerical results obtained from CFD are in close agreement with experimental wind tunnel test results.

Fiouz et al. [20] have conducted numerical investigation on single layer space struss structural member. The analysis was conducted for different types of rise-to-span ratios and dome types. The dome shapes considered for the analysis are schwedler and ribbed type.

Pere´ n et al. [21] have conducted numerical investigation of single-zone low rise building structures using techniques of CFD. The RANS average equation was used for analysis of single- span versus double-span leeward saw tooth roof geometries with varying opening rations i.e. convex type, straight type and concave type.

Abbas et al. [22] have conducted numerical investigation of masonry chimney using techniques of Computational Fluid Dynamics. The CFD investigation of masonry chimney was conducted in ANSYS software and variation of pressure with respect to chimney height is determined. The drag coefficient is determined for different fluid flow conditions as well.

Abdollah et. al. [23] Tall modern buildings are extremely sensitive to the wind. Thus, assessment of wind loads to design these buildings is essential. The purpose of this study is first to introduce a theoretical framework and simultaneously express basic aerodynamic studies. Furthermore, assessments are made to reduce drag coefficient performance of aerodynamic modification approaches including chamfered, rounded, and recessed corners as well as the performance of aerodynamic formations namely, set-back, taper, and 45-deg helical in a tall triangular building of about 120 m (40 stories). CFD simulation of this study is done by Autodesk Flow Design 2014. Building scales are presumed to be B = 1/6H. The results show that aerodynamic modification of rounded-corners, tapered are capable to cause a reduction in the drag coefficient of the building by 66% and 24%, respectively. Moreover, the technique of aerodynamic modification is approximately 74% more efficient to meet wind effect than aerodynamic form techniques.

Elshaer et. al. [24] The design of lateral load resisting systems in tall buildings is often determined by wind-induced loads and movements. The external contour of the structure is one of the many factors that affect the wind loading and responses in the design. The Building Corner Aerodynamic Optimization Process (AOP) described in this study is a methodology specifically developed to minimize the impact of wind on buildings. The achievement of this objective is facilitated by the utilization of several techniques in the AOP. These techniques include an optimization strategy, a large eddy simulation (LES), and an artificial neural network (ANN)-based surrogate model. Corner mitigation has a minimal effect on the architectural and structural design, as an example. Here, we showcase two instances of aerodynamic optimization techniques that have been developed to minimize drag and lift forces by integrating wind directionality and turbulence. The reduction in reactions to wind flow across the structure and along the building is observed to be more than 30% when a two-surface chamfering is restricted to 20% of the building width.

Aboshosha et. al. [25] An analysis is conducted on the aerodynamic behavior of a standard tall structure, known as the CAARC model, using Large Eddy Simulation (LES). The LES utilizes the Consistent Discrete Random Flow Generation (CDRFG) technique to generate the inflow boundary condition. This technique accurately represents the turbulence spectrum and coherency. The study investigates the aerodynamic characteristics of two different building configurations: a standalone building and a building with complex surrounding structures. The results are evaluated in comparison to those obtained from a previous wind tunnel investigation. The wind tunnel measurements and LES-derived calculations show a strong correlation in terms of pressure, wind-induced responses, top displacement, top acceleration, and base moments. The accuracy of the model is evidenced by the average disparity of 4% for pressures and 6% for dynamic reactions between LES and wind tunnel data in the simulated wind directions. The mean pressure coefficients and rms pressure coefficients of the isolated and complex surrounding configurations exhibited a difference of 50% and 40%, respectively, as expected. The LES model accurately predicts the responses of the study structure and the distribution of wind pressure in a timely manner. In the future, the use of computational fluid dynamics (CFD) in wind engineering applications is expected to be encouraged. Holmes et. al. [26] This study compares the projected along-wind base moments of a typical tall structure with the projections from the Australian/New Zealand Standard, the American Standard (ASCE 7), and the Hong Kong Code of Practice (2004). The forecasts are based on data obtained from multiple wind tunnels as part of an international benchmark study. The algorithms' forecasts exhibited notable disparities, as two of them produced values that were below the mean of the wind tunnel data. The drag coefficients for the building, as specified by the Hong Kong Code, are found to be considerably below the required threshold. This conclusion is supported by the measured effective drag coefficients and other relevant criteria. An apparent discrepancy in the numerator utilized for computing the gale impact factor for dynamic structures could potentially explain certain lower projections in ASCE 7. The crosswind base moments and resulting accelerations predicted by the Australian/New Zealand Standard were compared to the wind tunnel data. The predictions made by The Standard for the cross-wind moments and subsequent accelerations closely align with the upper limits and averages observed in the wind-tunnel data. This suggests that the comparisons between the predictions and the data are accurate.

Jørgensen et. al. [27] The comparison was made between the results obtained from wind tunnel experiments and simulations conducted using both a full Large Eddy Simulation (LES) and an embedded-LES (ELES) approach. The calculations were conducted using the commercial computational fluid dynamics (CFD) software ANSYS FLUENT. The reference length used for the computations was the height of the cube. Additionally, the Reynolds number (Reh) was determined to be 1.3x105. The objective of this study was to evaluate the accuracy of the time-averaged surface pressure on the cube, as well as the numerically simulated flow upstream and around it. In addition, this document will discuss the ELES's modeling of altering surface pressure. The computed average flow is found to be consistent with the wind tunnel data, even though the frequency spectrum of the upstream flow lacks low and high frequency components. The time-averaged surface pressures of the cube exhibit a wind load distribution along its streamwise centerline, as expected. The relative variations range from -16% to +18%. The data obtained from the front and rear of the cube is recorded with higher precision. However, the upper face of the cube exhibits significant inconsistencies due to the varying surface pressure caused by the ELES. Meroney et. al. [28] The widely accepted notion that computational fluid dynamics (CFD) and experimental fluid dynamics (EFD) are in a state of competition and conflict has persisted for almost five decades. The issue regarding the timeline for the closure of our physical modeling facilities was frequently brought up. The investigation does not acknowledge the significant synergistic benefits that arise from combining the most favorable characteristics of both Computational Fluid Dynamics (CFD) and Experimental Fluid Dynamics (EFD) as research and design methodologies. The integration of both Experimental Fluid Dynamics (EFD) and Computational Fluid Dynamics (CFD) in a hybrid management style enables the acceleration of the discovery process, improved understanding of flow phenomena, and often leads to reduced costs and shorter research durations. This study examines common concerns related to hybrid research or design approaches in the field of wind engineering and the constructed environment. The inherent risk involved in engineering judgments often leads to skepticism and reluctance to rely solely on "models," "simulations," or "virtual" reality for making design decisions. This statement holds true, especially when considering the possibility of severe consequences or loss of life that may occur if an incorrect response is chosen. Thus, it is always advisable to perform a thorough validation of our estimates by comparing them to real-life full-scale flow scenarios when extending our forecasts into unfamiliar areas. Engineers employ a systematic approach to examine each submodule of their design individually in complex, extensive, or time-consuming situations. This is done instead of conducting comprehensive testing all at once.

Derickson et. al. [29] The use of numerical modeling in wind engineering is essential for accurately predicting meteorological and climatic conditions, despite the skepticism and derision it may face. This paper presents an analysis of the development of computational fluid dynamics (CFD) in the field of computational wind engineering (CWE), including both successful and unsuccessful applications. The main focus of the examination will be on the practical use of Computational Fluid Dynamics (CFD) in the context of buildings and other structures. Computational fluid dynamics (CFD) is utilized by snow researchers as a supplementary approach to compute snow accumulation. Several hypotheses have been proposed to explain the formation of drifting and the movement of snow. The drift flux model developed by Bang et al. has been successfully integrated into the

commercial software Flow-3D. The relative motions in this model are governed by drag forces, which are regulated by pressure gradients, and the two phases of the air and snow combination. The occurrence of this phenomenon is attributed to a situation where the threshold of friction velocity required for snow mobility is lower than the air shear force exerted on the ground surface. As a consequence, snow accumulates in certain areas. The researchers utilized a basic FAE computer model to assess the deposition or ablation of snow in a grid of small regions. The wind data from meteorological sources was utilized in conjunction with other data to estimate the airflow patterns around a physical structure located at the South Pole. The task was completed by utilizing a three-dimensional computational fluid dynamics code called TASCflow. One alternative approach is to utilize a Computational Fluid Dynamics (CFD) solver, such as FLUENT, for the purpose of calculating the wind field and turbulence. The computation of particle trajectories and their subsequent impact and deposition on ground surfaces can be achieved by utilizing a Lagrangian discrete particle motion solver. The capability to predict the trajectories of descending particles within the wind field is provided.

Nozu et. al. [30] The focus of this investigation is on the application of large eddy simulation (LES) in metropolitan environments to design structures that can withstand high winds. Our company provides the unstructured grid approach, which allows for accurate calculation of wind pressures and forces on complex structures. This approach is based on the open-source CFD code. The Large Eddy Simulation (LES) approach is utilized to model the flow in an urban setting, specifically emphasizing the safety of a tall building when subjected to wind loads. The examination of the aerodynamic characteristics is conducted by utilizing the combined model. The employed method utilizes overset grids, which consist of both Cartesian and unstructured grids. The capability of accurately reproducing the intricate patterns of the near-wake flows around a specific building in a highly populated area has been demonstrated in previous research using the unstructured grid methodology. The turbulent structures within the urban canopy can be effectively simulated using the Cartesian grid method. The wind force acting on a tall urban skyscraper was accurately determined using a hybrid model consisting of a Cartesian grid and an unstructured grid. There is a widely held belief that the wind affects a tall structure located along a street in varying ways based on its height, particularly when the wind is blowing towards the main roads. As a result, there is an increased probability of the existence of a substantial torsional force. The veracity of the findings is confirmed by conducting wind tunnel experiments. The assessment of the structural stability of a tall structure involves the calculation and examination of wind force coefficients and wind pressure distributions on its surfaces.

Yoshikawa et. al. [31] This paper aims to present and discuss the key factors that need to be taken into account when utilizing computational fluid dynamics (CFD) simulations to evaluate the effects of wind on tall structures. An analysis of the major parameters of the atmospheric boundary layer is conducted to evaluate the accuracy of the upstream wind flow in a numerical simulation. There are four fundamental methods that can be used to establish the inflow boundary conditions. Currently, an evaluation is underway to assess the strengths and limitations of the latest and potential methodologies. The CAARC architecture involves the evaluation of experimental and numerical data through comparisons. Significant discrepancies were observed between the computer models and the

wind tunnel experiments. When comparing results, it is crucial to ensure that the inflow boundary conditions are identical. Any discrepancies in these conditions can lead to significant inaccuracies. The latest findings from the benchmark research suggest that the results show promise and become increasingly accurate as the information is enhanced. There is a significant need for a standardized recommendation on the use of Computational Fluid Dynamics (CFD) Large Eddy Simulation (LES) for calculating wind loads in structural design. This need arises from the inconsistencies in data analysis observed in various research studies. The paper concludes by providing a discussion on the core areas of study that are crucial for future research.

Zhang et. al. [32] The objective of this research is to investigate the vibration caused by wind in the CAARC standard tall building model using a combination of structural modal analysis and turbulent computational fluid dynamics (CFD). The numerical procedure utilizes an artificial inflow turbulence generation method to accurately simulate the naturally unstable airflow in the atmospheric boundary layer. The Zonal Detached-Eddy Simulation (ZDES) utilizes its second mode to effectively simulate turbulent flow. To transfer unstable loads from fluid nodes to structure nodes, a conservative quadrature-projection approach is employed. The aerodynamic attenuation in the fluid-structure interaction process is determined by empirical functions. The derivation of these functions is based on wind tunnel experiments. The flow solutions and structural responses are compared to experimental findings in terms of average and root mean square values, considering a wide range of reduced velocities. The importance of turbulent inflow conditions and aeroelastic effects is emphasized. The present methodology possesses the capability to serve as an initial design tool for evaluating the influence of turbulent wind on tall structures, as it generates predictions with a notable level of accuracy.

3. Research Methodology/Experimental

4.1 Methodology Flow Chart

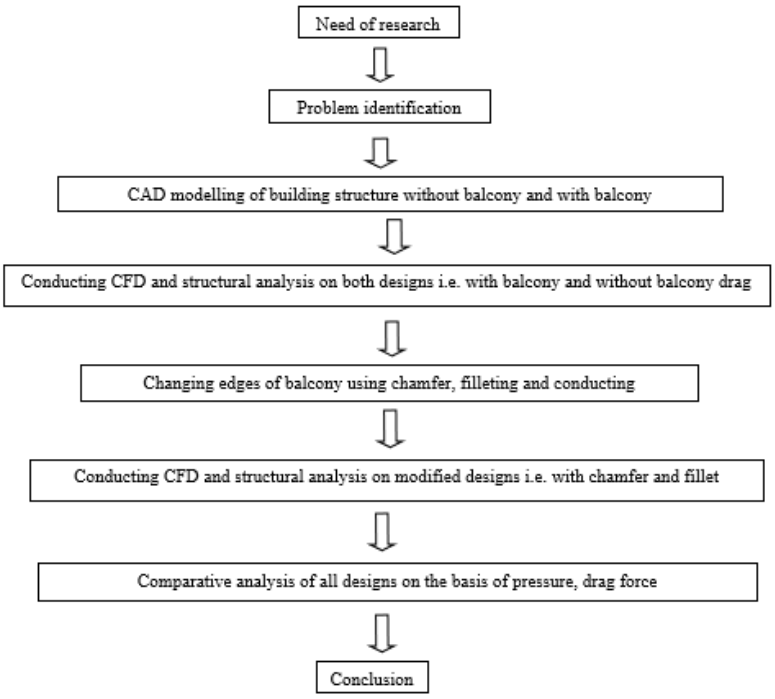

4.2 Methodology Steps

The methodology for FEA analysis involves various steps which includes pre-processin, solution and post-processing stage.

4.2.1 CAD Modelling

The design of building is developed in design software. The 1st design is sharp edged building. The model is developed using sketch and extrude tool. The developed design of sharp edged chimney is shown in figure 4.1. The dimensions of building are taken from the literature [23]. The height of the building was H = 120 m (about 40 stories) and the width was 21 m. The proportions of the models are B/H = 1/6.

Table 4.1: Dimensions of building

Height of building	120m
Number of stories	40
Width of base	20m

4.2.2 Importing CAD model

The design of chimney is imported in ANSYS design modeller. In the modeller the building design is tested for hard edges, surface imperfections or any other defects as shown in figure 4.6.

4.2.3 Enclosure Modelling

The enclosure surrounding the building is developed as shown in figure 4.7 below. The enclosure of 150m * 150m * 150m is developed covering ample space. The chimney design with enclosure is shown in figure 5.7 below.

4.2.4 Meshing

The model of building is discretized using tetrahedral element type. The growth rate for meshing is set to 1.2. The inflation is set to normal. The geometry doesn't have topological consistency and therefore it is meshed with tetrahedral element type.

The model is meshed and the number of elements generated is 195831 whereas the number of nodes generated is 37924.

4.2.5 Loads and Boundary Condition

The domain is defined for computation. The computational domain includes for chimney and for air. For chimney the domain type is set to solid and material is set to concrete type. The domain motion is set to stationary.

The domain is defined for the fluid. The fluid domain material is set to air with reference pressure is set to 1atm. The thermal energy model is set to isothermal. The air inlet boundary condition is defined as shown in figure 4.11 below. The air inlet magnitude defined is 44m/s as per IS:875 (zone 3).

The air outlet boundary conditions are defined. The outlet boundary condition defined is relative pressure with 0 Pa magnitude. The turbulence intensity is set to 5%.

Aspects of Wind Load Analysis:

1. The effect of wind load on structure is different for each location of chimney structure.
2. The inlet air velocity profile is uniform for CFD simulation.
3. The velocity is taken as per IS: 875 code.
4. The standard k-epsilon turbulence model is used for the analysis which gives reasonably good fluid flow prediction and is easy to run.

4.2.6 Solver Settings

The solver settings are defined which include RMS residual values. The RMS residual target is set to .0001 and number of iterations are defined to 100.

4.2.7 Fluid Structure Interaction

The solver settings are defined which include RMS residual values. The RMS residual target is set to .0001 and number of iterations are defined to 100. The pressure value obtained from CFD analysis is mapped on to building structure and static structural analysis is run. From the static structural analysis, the lateral deformation and shear stress is obtained. The mapped pressure plot for FSI analysis is shown in figure 4.13.

The pressure value obtained from the CFD analysis is mapped on to building surface which tends to cause lateral deformation. The base of the building is applied with fixed support as shown above.

4.2.8 Solution Stage

The RMS residual values of each variable are determined for mass, momentum and energy values. The final result has shown convergence of all the 3 variables with 70 iterations.

Solver Report

“OUTER LOOP ITERATION = 29 CPU SECONDS = 2.044E+02

```
 ------------------------------------------------------------------------
|      Equation      | Rate | RMS Res | Max Res |  Linear Solution |
+--------------------+------+---------+---------+------------------+
| U-Mom              | 0.95 | 1.0E-04 | 1.2E-02 |      6.9E-02  OK|
| V-Mom              | 0.93 | 1.5E-05 | 2.5E-03 |      8.8E-02  OK|
| W-Mom              | 0.95 | 1.3E-05 | 1.3E-03 |      7.3E-02  OK|
| P-Mass             | 0.88 | 7.7E-06 | 5.6E-04 |  4.7  9.4E-02  OK|
+--------------------+------+---------+---------+------------------+
| K-TurbKE           | 1.00 | 1.8E-04 | 2.8E-02 |  5.4  4.6E-05  OK|
| E-Diss.K           | 0.92 | 3.1E-05 | 4.4E-03 |  7.3  1.0E-04  OK|
```

```
+---------------------+------+---------+---------+-----------------+
==========================================================================
OUTER LOOP ITERATION =   30                CPU SECONDS = 2.115E+02
-------------------------------------------------------------------
|      Equation       | Rate | RMS Res | Max Res |  Linear Solution |
+---------------------+------+---------+---------+-----------------+
| U-Mom               | 0.95 | 9.9E-05 | 1.2E-02 |       7.0E-02  OK|
| V-Mom               | 0.90 | 1.3E-05 | 2.2E-03 |       9.0E-02  OK|
| W-Mom               | 0.96 | 1.3E-05 | 1.3E-03 |       7.3E-02  OK|
| P-Mass              | 0.89 | 6.9E-06 | 5.0E-04 |  4.7  9.9E-02  OK|
+---------------------+------+---------+---------+-----------------+
| K-TurbKE            | 0.97 | 1.7E-04 | 2.8E-02 |  5.4  4.8E-05  OK|
| E-Diss.K            | 0.93 | 2.9E-05 | 4.1E-03 |  7.3  1.2E-04  OK|
+---------------------+------+---------+---------+-----------------+
CFD Solver finished: Sun Apr 04 18:02:19 2021
CFD Solver wall clock seconds: 2.1505E+02
==========================================================================
          Termination and Interrupt Condition Summary
==========================================================================
CFD Solver: All target criteria reached
  (Equation residuals)
==========================================================================
          Boundary Flow and Total Source Term Summary
==========================================================================
+--------------------------------------------------------------+
|                    U-Mom-air domain                          |
+--------------------------------------------------------------+
Boundary       : Default Fluid Solid Interface Side 1   -2.8515E+05
Boundary       : air domain Default                     -1.9355E+05
Boundary       : air in                                  5.0501E+07
Boundary       : opening                                -5.0035E+07
```

Domain Imbalance : -1.3428E+04

+----------+

| V-Mom-air domain |

+----------+

Boundary : Default Fluid Solid Interface Side 1 4.5192E+03

Boundary : air domain Default -4.8658E+03

Boundary : air in 5.5772E-06

Boundary : opening 2.2931E+02

Domain Imbalance : -1.1724E+02

+----------+

| W-Mom-air domain |

+----------+

Boundary : Default Fluid Solid Interface Side 1 -2.1717E+03

Boundary : air domain Default 8.5578E+02

Boundary : air in -5.2289E-04

Boundary : opening 2.0945E+03

Domain Imbalance : 7.7850E+02

+----------+

| P-Mass-air domain |

+----------+

Boundary : air in 1.1895E+06

Boundary : opening -1.1896E+06

Domain Imbalance : -5.3750E+00

+----------+

| Normalised Imbalance Summary |

+----------+

| Equation | Maximum Flow | Imbalance (%) |

+----------+

U-Mom-air domain	5.0501E+07	-0.0266
V-Mom-air domain	5.0501E+07	-0.0002
W-Mom-air domain	5.0501E+07	0.0015
P-Mass-air domain	1.1896E+06	-0.0005

Wall Force and Moment Summary

Pressure Force On Walls			
	X-Comp.	Y-Comp.	Z-Comp.
Domain Group: air domain			
Default Fluid Solid Interface Si	2.8459E+05	-4.5056E+03	2.1140E+03
air domain Default	0.0000E+00	4.8720E+03	-9.3218E+02
Domain Group Totals :	2.8459E+05	3.6632E+02	1.1818E+03

Viscous Force On Walls			
	X-Comp.	Y-Comp.	Z-Comp.
Domain Group: air domain			
Default Fluid Solid Interface Si	5.5720E+02	-1.3584E+01	5.7713E+01
air domain Default	1.9355E+05	-5.8997E+00	7.6268E+01
Domain Group Totals :	1.9411E+05	-1.9484E+01	1.3398E+02

Pressure Moment On Walls			
	X-Comp.	Y-Comp.	Z-Comp.
Domain Group: air domain			

Default Fluid Solid Interface Si 8.1024E+04 5.7138E+06 -3.6667E+02
air domain Default -4.6528E+05 -1.6014E+07 7.8225E+03
---------- ---------- ----------
Domain Group Totals : -3.8425E+05 -1.0300E+07 7.4558E+03

+----------+
| Viscous Moment On Walls |
+----------+

X-Comp. Y-Comp. Z-Comp.
Domain Group: air domain
Default Fluid Solid Interface Si 4.1492E+01 6.4337E+03 1.6457E+01
air domain Default 3.9404E+02 1.4069E+07 2.4610E+04
---------- ---------- ----------
Domain Group Totals : 4.3553E+02 1.4076E+07 2.4627E+04

+----------+
| Locations of Maximum Residuals |
+----------+

Equation	Domain Name	Node Number
U-Mom	air domain	107014
V-Mom	air domain	105310
W-Mom	air domain	23537
P-Mass	air domain	108475
K-TurbKE	air domain	5629
E-Diss.K	air domain	105307
K-TurbKE-air domain	Auto Timescale	3.65382E+01
E-Diss.K-air domain	Auto Timescale	3.65382E+01

```
+-------------------------------------------------------------------+
|                  Average Scale Information                        |
+-------------------------------------------------------------------+
Domain Name : air domain
   Global Length                          = 1.7051E+02
   Minimum Extent                         = 1.4500E+02
   Maximum Extent                         = 2.0600E+02
   Density                                = 1.1765E+00
   Dynamic Viscosity                      = 1.8310E-05
   Velocity                               = 4.1864E+01
   Advection Time                         = 4.0730E+00
   Reynolds Number                        = 4.5868E+08
   Speed of Sound                         = 3.4728E+02
   Mach Number                            = 1.2055E-01
Domain Name : chimney
   Global Length                          = 9.8132E+00
   Minimum Extent                         = 6.0000E+00
   Maximum Extent                         = 4.5000E+01
   Density                                = 2.3000E+03
+-------------------------------------------------------------------+
|                  Variable Range Information                       |
+-------------------------------------------------------------------+
Domain Name : air domain
+-------------------------------------------------------------------+
|     Variable Name                      |    min    |    max    |
+-------------------------------------------------------------------+
| Density                                |  1.16E+00 |  1.19E+00 |
| Specific Heat Capacity at Constant Pressure|  1.00E+03 |  1.00E+03 |
| Dynamic Viscosity                      |  1.83E-05 |  1.83E-05 |
| Thermal Conductivity                   |  2.61E-02 |  2.61E-02 |
| Isothermal Compressibility             |  9.76E-06 |  9.97E-06 |
```

Static Entropy	3.14E+00	9.27E+00
Velocity u	-2.16E+01	4.67E+01
Velocity v	-1.55E+01	1.66E+01
Velocity w	-1.03E+01	7.61E+00
Pressure	-1.07E+03	1.09E+03
Turbulence Kinetic Energy	1.64E-11	4.97E+01
Turbulence Eddy Dissipation	8.47E-11	5.43E+05
Eddy Viscosity	2.60E-13	1.93E+00
Temperature	3.00E+02	3.00E+02

Domain Name : chimney

Variable Name	min	max
Density	2.30E+03	2.30E+03
Specific Heat Capacity at Constant Pressure	8.80E+02	8.80E+02
Thermal Conductivity	1.40E+00	1.40E+00
Static Entropy	5.44E+00	5.44E+00
Temperature	3.00E+02	3.00E+02
Static Enthalpy	1.63E+03	1.63E+03

CPU Requirements of Numerical Solution

Subsystem Name	Discretization (secs. %total)	Linear Solution (secs. %total)
Momentum and Mass	1.18E+02 53.6 %	1.23E+01 5.6 %
TurbKE and Diss.K	3.92E+01 17.7 %	2.02E+01 9.1 %
Subsystem Summary	1.58E+02 71.3 %	3.25E+01 14.7 %
GGI Intersection	2.20E-02 0.0 %	

File Reading	1.00E-01	0.0 %
Variable Updates	2.42E+01	10.9 %
File Writing	1.84E+00	0.8 %
Miscellaneous	4.88E+00	2.2 %
Total	2.21E+02”	

4. Results and Discussion

5.1 Sharp edged results

The CFD analysis is conducted on sharp edged building structure to determine pressure and drag force acting on the structure. The analysis is conducted at 44m/s air speed and at 47m/s air speed.

5.1.1 Sharp Edged Geometry at 44m/s

The maximum pressure is obtained on windward side of the building wherein the pressure is 1195Pa. The pressure is lower on the leeward side of the building. The pressure difference tends to deform the structure and induce stress.

The maximum drag force is observed at the bottom center region of triangular face geometry as shown in red colored region. The maximum drag force obtained from the analysis is 9119N.

5.1.2 Triangular Geometry at 47m/s

The maximum pressure is obtained on windward side of the building wherein the pressure is 1364Pa. The pressure is lower on the leeward side of the building. The pressure difference tends to deform the structure and induce stress.

The maximum drag force is observed at the bottom canter region of triangular face geometry as shown in red coloured region. The maximum drag force obtained from the analysis is 10410N.

5.1.3 FSI Studies of Triangular Geometry at 47m/s

The fluid structure interaction studies are conducted on structure as shown in figure 6.5. From the FSI studies the lateral deformation and shear stress induced on the structure is determined.

From the FSI studies, the maximum deformation is obtained at the top free end of building structure. The magnitude of maximum deformation obtained is 8.9895mm.

The shear stress distribution plot is obtained from the FSI studies as shown in figure 5.6 above. The maximum shear stress obtained from the analysis is .00966MPa.

5.2 Rounded edged results

The CFD analysis is conducted on rounded edged building structure to determine pressure and drag force acting on the structure. The analysis is conducted at 44m/s air speed and at 47m/s air speed.

5.2.1 Rounded Edged Geometry at 44m/s

The maximum pressure is obtained on windward side of the building wherein the pressure is 1211Pa. The pressure is lower on the leeward side of the building. The pressure difference tends to deform the structure and induce stress.

The maximum drag force is observed at the bottom center region of triangular face geometry as shown in red colored region. The maximum drag force obtained from the analysis is 3826N.

5.2.2 Rounded Edged Geometry at 47m/s

The maximum pressure is obtained on windward side of the building wherein the pressure is 1382Pa. The pressure is lower on the leeward side of the building. The pressure difference tends to deform the structure and induce stress.

The maximum drag force is observed at the bottom canter region of triangular face geometry as shown in red coloured region. The maximum drag force obtained from the analysis is 43650N.

5.2.3 FSI Studies of Rounded Edged Geometry at 47m/s

The fluid structure interaction studies are conducted on structure as shown in figure 5.11. From the FSI studies the lateral deformation and shear stress induced on the structure is determined.

From the FSI studies, the maximum deformation is obtained at the top free end of building structure. The magnitude of maximum deformation obtained is 9.2839mm.

The shear stress distribution plot is obtained from the FSI studies as shown in figure 5.12 above. The maximum shear stress obtained from the analysis is .00959MPa.

5.3 Rounded Triangular Geometry with Balcony Results

The CFD analysis is conducted on rounded edged building structure with balcony to determine pressure and drag force acting on the structure. The analysis is conducted at 44m/s air speed and at 47m/s air speed.

5.3.1 Rounded Edged Geometry with balcony at 44m/s

The maximum pressure is obtained on windward side of the building wherein the pressure is 1209Pa. The pressure is lower on the leeward side of the building. The pressure difference tends to deform the structure and induce stress.

The maximum drag force is observed at the bottom center region of triangular face geometry as shown in red colored region. The maximum drag force obtained from the analysis is 3588N.

5.3.2 Rounded Edged Geometry with balcony at 47m/s

The maximum pressure is obtained on windward side of the building wherein the pressure is 1380Pa. The pressure is lower on the leeward side of the building. The pressure difference tends to deform the structure and induce stress.

The maximum drag force is observed at the bottom canter region of triangular face geometry as shown in red coloured region. The maximum drag force obtained from the analysis is 40940N.

5.3.3 FSI Studies of Rounded Edged Geometry with balcony at 47m/s

The fluid structure interaction studies are conducted on structure as shown in figure 5.17. From the FSI studies the lateral deformation and shear stress induced on the structure is determined.

From the FSI studies, the maximum deformation is obtained at the top free end of building structure. The magnitude of maximum deformation obtained is 8.253mm.

The shear stress distribution plot is obtained from the FSI studies as shown in figure 5.18 above. The maximum shear stress obtained from the analysis is .02939MPa.

5.4 Rounded Triangular Geometry with Rounded Balcony Results

The CFD analysis is conducted on rounded edged building structure with balcony to determine pressure and drag force acting on the structure. The analysis is conducted at 44m/s air speed and at 47m/s air speed.

5.4.1 Rounded Edged Geometry with Rounded Balcony at 44m/s

The maximum pressure is obtained on windward side of the building wherein the pressure is 1210Pa. The pressure is lower on the leeward side of the building. The pressure difference tends to deform the structure and induce stress.

The maximum drag force is observed at the bottom center region of triangular face geometry as shown in red colored region. The maximum drag force obtained from the analysis is 4133N.

5.4.2 Rounded Edged Geometry with Rounded balcony at 47m/s

The maximum pressure is obtained on windward side of the building wherein the pressure is 1210Pa. The pressure is lower on the leeward side of the building. The pressure difference tends to deform the structure and induce stress.

The maximum drag force is observed at the bottom canter region of triangular face geometry as shown in red coloured region. The maximum drag force obtained from the analysis is 4133N.

5.4.3 FSI Studies of Rounded Edged Geometry with Rounded balcony at 47m/s

The fluid structure interaction studies are conducted on structure as shown in figure 5.23. From the FSI studies the lateral deformation and shear stress induced on the structure is determined.

From the FSI studies, the maximum deformation is obtained at the top free end of building structure. The magnitude of maximum deformation obtained is 6.2763mm.

The shear stress distribution plot is obtained from the FSI studies as shown in figure 5.24 above. The maximum shear stress obtained from the analysis is .02193MPa.

5.5 Rounded Triangular Geometry with Rounded Balcony Results

The CFD analysis is conducted on rounded edged building structure with balcony to determine pressure and drag force acting on the structure. The analysis is conducted at 44m/s air speed and at 47m/s air speed.

5.5.1 Rounded Edged Geometry with Rounded Balcony at 44m/s

The maximum pressure is obtained on windward side of the building wherein the pressure is 1210Pa. The pressure is lower on the leeward side of the building. The pressure difference tends to deform the structure and induce stress.

The maximum drag force is observed at the bottom center region of triangular face geometry as shown in red colored region. The maximum drag force obtained from the analysis is 4133N.

5.5.2 Rounded Edged Geometry with Rounded balcony at 47m/s

The maximum pressure is obtained on windward side of the building wherein the pressure is 1210Pa. The pressure is lower on the leeward side of the building. The pressure difference tends to deform the structure and induce stress.

The maximum drag force is observed at the bottom canter region of triangular face geometry as shown in red coloured region. The maximum drag force obtained from the analysis is 4133N.

5.5.3 FSI Studies of Rounded Edged Geometry with Rounded balcony at 47m/s

The fluid structure interaction studies are conducted on structure as shown in figure 5.29. From the FSI studies the lateral deformation and shear stress induced on the structure is determined.

From the FSI studies, the maximum deformation is obtained at the top free end of building structure. The magnitude of maximum deformation obtained is 6.2763mm.

The shear stress distribution plot is obtained from the FSI studies as shown in figure 5.30 above. The maximum shear stress obtained from the analysis is .02193MPa.

5.6 Rounded Triangular Geometry with Opening Results

The CFD analysis is conducted on rounded edged building structure with opening to determine pressure and drag force acting on the structure. The analysis is conducted at 44m/s air speed and at 47m/s air speed.

5.6.1 Rounded Edged Geometry with Opening at 44m/s

The maximum pressure is obtained on windward side of the building wherein the pressure is 1216Pa. The pressure is lower on the leeward side of the building. The pressure difference tends to deform the structure and induce stress.

The maximum drag force is observed at the bottom center region of triangular face geometry as shown in red colored region. The maximum drag force obtained from the analysis is 3502N.

5.6.2 Rounded Edged Geometry with Opening at 47m/s

The maximum pressure is obtained on windward side of the building wherein the pressure is 1388Pa. The pressure is lower on the leeward side of the building. The pressure difference tends to deform the structure and induce stress.

The maximum drag force is observed at the bottom canter region of triangular face geometry as shown in red coloured region. The maximum drag force obtained from the analysis is 3996N.

5.6.3 FSI Studies of Rounded Edged Geometry with Opening at 47m/s

The fluid structure interaction studies are conducted on structure as shown in figure 5.35. From the FSI studies the lateral deformation and shear stress induced on the structure is determined.

From the FSI studies, the maximum deformation is obtained at the top free end of building structure. The magnitude of maximum deformation obtained is 6.362mm.

The shear stress distribution plot is obtained from the FSI studies as shown in figure 5.36 above. The maximum shear stress obtained from the analysis is .01531MPa.

5.7 Comparative Studies

The comparative studies are conducted between different designs of building structure on the basis of pressure, lateral deformation and shear stress. The pressure comparison is made at different velocities i.e. 10m/s, 44m/s and 47m/s. The pressure comparison plot is shown in table 5.1 below.

Table 5.1: Pressure Comparison for different designs

Design Type	Max Pressure@ 10m/s	Max Pressure@ 44m/s	Max Pressure@47 m/s
Triangular shape	61.77	1195	1364
Rounded Triangular Edge without opening	62.58	1211	1382
Rounded Triangular Edge with Balconies	62.5	1209	1380
Rounded Triangular Edge with Rounded Balconies	62.56	1210	1210
Rounded Triangular Edge with opening	62.85	1216	1388

The pressure comparison plot shows increase in induced pressure on building structure with higher wind speeds. The maximum induced pressure is obtained for 47m/s air speed. The edge treatment has significant effect on reduction of induced pressure. At 47m/s air speed, the minimum induced pressure is obtained for Rounded Triangular Edge with Rounded Balconies design type.

Table 5.2: Fluid Structure Interaction (FSI) studies comparison

Design Type	Deformation (mm)	Shear stress (Mpa)
Triangular shape	8.9895	0.00966
Rounded Triangular Edge without opening	9.283	0.00959
Rounded Triangular Edge with Balconies	8.253	0.0293
Rounded Triangular Edge with Rounded Balconies	6.276	0.02193
Rounded Triangular Edge with opening	6.362	0.0153

The fluid structure interaction (FSI) studies are conducted on different design configuration of building structure. The comparative plot has shown that

5. Conclusions

The CFD analysis is conducted on chimney as per IS:875 zone 3 conditions. The induced pressure, drag force and velocity fields are evaluated across the chimney with different shapes i.e. triangular sharp edges, rounded triangular edges, rounded triangular edge with opening, rounded triangular edges with balconies and rounded triangular edges with rounded balconies. The fluid structure interaction (FSI) studies are conducted using m25 concrete. The detailed findings are summarized below:

1. The lateral deformation is observed to increase with increase in chimney height.
2. The presence of opening in building structure enabled to reduce the drag force induced on the building structure.
3. The opening type of building structure has 29.23% lower deformation as compared to sharp edged building structure.
4. The building structure with rounded balconies has shown lower induced pressure as compared to sharp edged balconies.
5. The building structure with rounded balconies has shown 12.82% lower induced pressure as compared to sharp edged balconies. The lower induced pressure would tend to induces lower lateral deformation.
6. The incorporation of balconies on the structure have caused an increase in induced pressure.
7. The rounded structure with sharp edged balconies has shown 1.17% increase in induced pressure as compared to sharp edged structure without balconies.
8. The incorporation of balconies resulted in increased of shear stress at the base.
9. The base shear induced on structure with balconies is double the base shear induced on structure without balconies.
10. The presence of balconies on the structure tends to increase the distance between the wall of building structure and low pressure zone and thereby reducing the effect of low pressure on building structure.

References:

[1] [1] A E. Hassaballa, Fathelrahman M. Adam., M. A. Ismaeil, "Seismic Analysis of a Reinforced Concrete Building by Response Spectrum Method", IOSR Journal of Engineering (IOSRJEN),Vol. 3, Issue 9 (September. 2013),PP 01-09.

[2] [2] Kavita K. Ghogare, "Seismic Analysis & Design of RCC Building", International Journal of Research in Advent Technology, Vol.3, No.2, February 2015.

[3] [3] Gaurav Kumar, MeghaKalra, "Review Paper On Seismic Analysis Of RCC Frame Structures With Floating Columns" , International journal of advanced technology in engineering and science, Vol. No.4, Special Issue No. 01, February 2016.

[4] [4]Gauri G. Kakpure, Ashok R. Mundhada, "Comparative Study of Static and Dynamic Seismic Analysis of Multistoried RCC Building by ETAB: A Review", International Journal of Emerging Research in Management &Technology, Volume-5, Issue-12, December 2016.

[5] [5]GouravSachdeva, PhrangkuparThabah, ErictonNonkyngynrih, "Analysis & behavior of RC Building Frame with Different Locations of Floating Columns", International Journal of Innovative Research in Science, Engineering and Technology, Vol. 5, Issue 6, June 2016.

[6] [6] K VenuManikanta, Dr. DumpaVenkateswarlu, "Comparative Study On Design Results Of A Multi-Storied Building Using STAAD Pro And ETABS For Regular And Irregular Plan Configuration", International Journal of Research Sciences and Advanced Engineering, Volume 2, Issue 15, PP: 204 - 215, September' 2016.

[7] [7] Ashok kumar N, Navaneethan M, Naviya B, Gopalakrishnan D, "Planning, Analysis & Design of Hospital Building Using Staad Prov8i", International Journal of Scientific & Engineering Research, Volume 8, Issue 4, April-2017.

[8] [8] B. GireeshBabu, "Seismic Analysis and Design of G+7 Residential Building Using STAADPRO", International Journal Of Advance Research, Ideas And Innovations In Technology, Volume3, Issue3, 2017

[9] [9] Harman, Hemant sood, "Analyzing the Effect of Cross-Sectional Change of Column on Symmetrical R.C.C. Frame Structure" International Journal of Engineering Research & Technology (IJERT), Vol. 6 Issue 06, June - 2017.

[10] [10] Mahesh Ram Patel, R.C. Singh, "Analysis of a tall structure using STAAD pro providing different wind intensities as per 875 Part-III", International Journal of Engineering Sciences & Research Technology, May, 2017

[11] [11] G. Guruprasad and G. Srikanth, "Seismic Evaluation of Irregular Structures" International Journal of Research in Advanced Engineering Technologies (IJRAET), Vol. 6 Issue 2, pp. 26-35, 2017.

[12] [12] AthulyaUllas and Nimisha P, "Response of Buildings of Different Plan Shapes Subjected To Wind Vibrations" International Research Journal of Engineering and Technology (IRJET), Vol. 4 Issue 5, pp. 1625-1628, 2017.

[13] [13] Pradeep Pujar and Amaresh, "Seismic Analysis of Plan Irregular Multi-Storied Building with and Without Shear Walls" International Research Journal of Engineering and Technology (IRJET), Vol. 4 Issue 8, pp. 1405-1411, 2017.

[14][14] Aniket A. Kale and S. A. Rasal, “Wind & Seismic Analysis of Multi-storey Building” International Journal of Emerging Research in Management & Technology, Vol. 6 Issue 5, pp. 25-30, 2017.

[15][15] **Abdollah et. al.** Tall modern buildings are extremely sensitive to the wind. Thus, assessment of wind loads to design these buildings is essential. The purpose of this study is first to introduce a theoretical framework and simultaneously express basic aerodynamic studies. Furthermore, assessments are made to reduce drag coefficient performance of aerodynamic modification approaches including chamfered, rounded, and recessed corners as well as the performance of aerodynamic formations namely, set-back, taper, and 45-deg helical in a tall triangular building of about 120 m (40 stories).

Figure captions

1. **Figure 1.1:** Assessment of pedestrian wind comfort [36]
2. **Figure 1.2:** Prediction of natural ventilation [38]
3. **Figure 1.3:** Investigation of HVAC system for indoor environment [39]
4. **Figure 1.4:** Prediction of pollutant dispersion [40]
5. **Figure 1.5:** Architectural design process with CFD simulation [37]
6. **Figure 2.1:** Schematic view of gable roof model [8]
7. **Figure 2.2:** Gable roof domain dimensions and meshes [8]
8. **Figure 4.1:** CAD design of sharp-edged building [23]
9. **Figure 4.2:** CAD design of filleted edged building [23]
10. **Figure 4.3:** CAD design of filleted edged building with opening [23]
11. **Figure 4.4:** CAD design of rounded building with sharp-edged balcony [23]
12. **Figure 4.5:** CAD design of rounded building with round-edged balcony [23]
13. **Figure 4.6:** Imported CAD design of building [23]
14. **Figure 4.7:** Enclosure modeling [23]
15. **Figure 4.8:** Meshed model [23]
16. **Figure 4.9:** Domain definition for concrete [23]
17. **Figure 4.10:** Domain definition for air [23]
18. **Figure 4.11:** Air inlet boundary condition [23]
19. **Figure 4.12:** Air outlet boundary condition [23]
20. **Figure 4.13:** Mapped pressure on building [23]
21. **Figure 5.1:** Pressure plot on Triangular Geometry @ 44m/s [23]
22. **Figure 5.2:** Drag force plot on Triangular Geometry @ 44m/s [23]

Line graphs

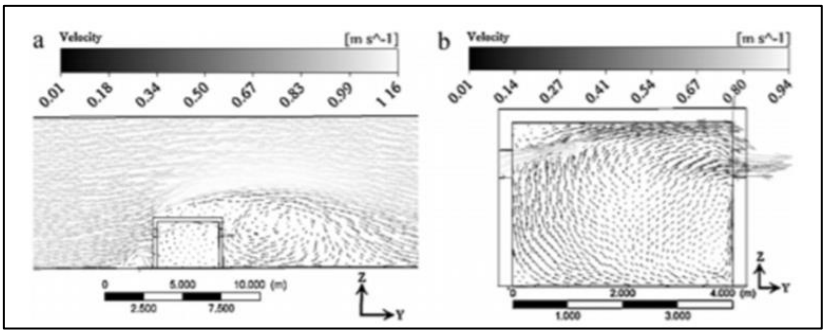

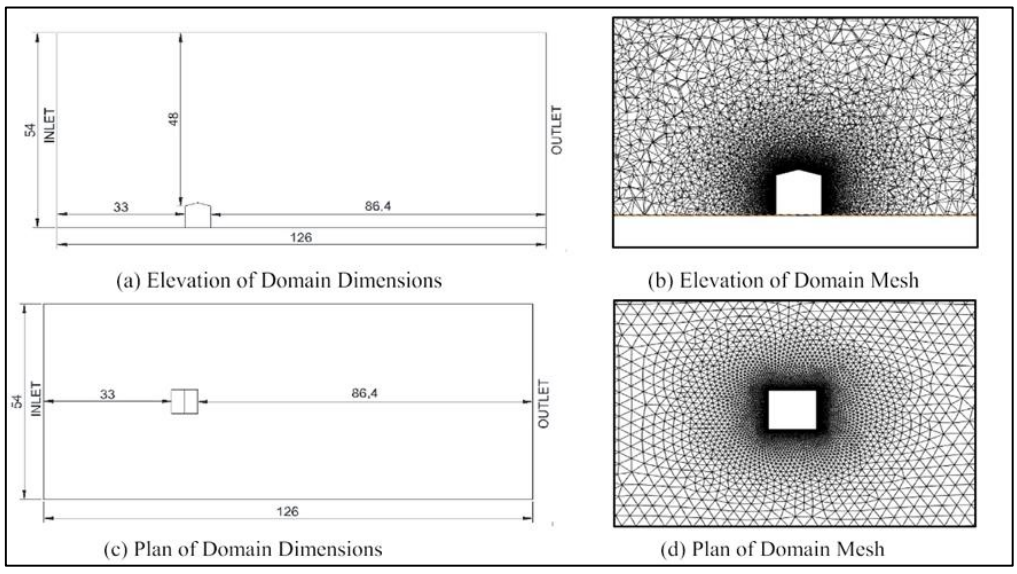

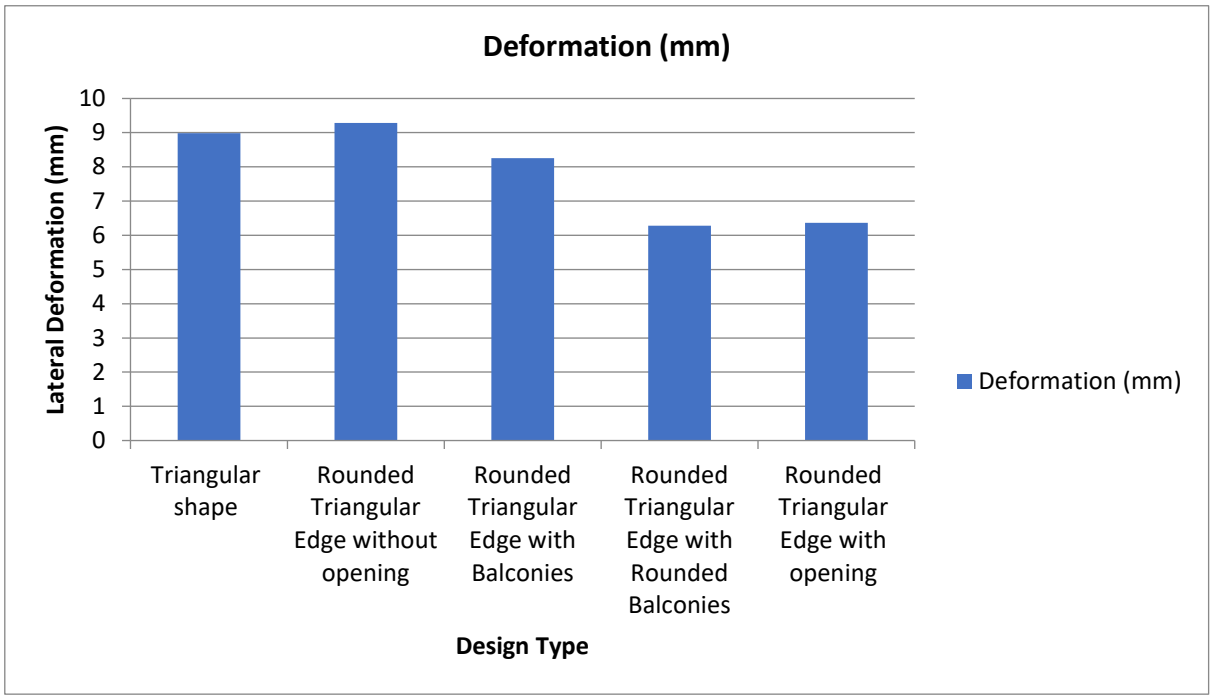
Deformation (mm)
Lateral Deformation (mm)
10
9
8
7
6
5
4
3
2
1
0
Triangular shape
Rounded Triangular Edge without opening
Rounded Triangular Edge with Balconies
Rounded Triangular Edge with Rounded Balconies
Rounded Triangular Edge with opening
Design Type
Deformation (mm)

Figures

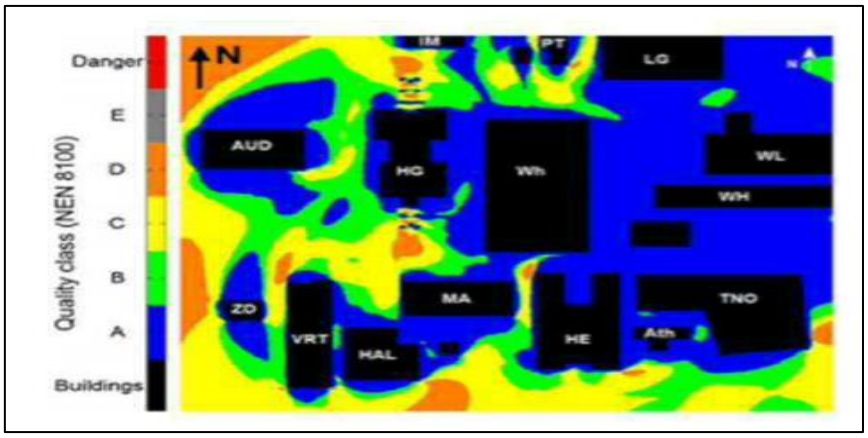
Danger
E
D
C
B
A
Buildings
Quality class (NEN 8100)
N
AUD
HG
Wh
WL
WH
LG
PT
ZD
VRT
HAL
MA
HE
Ath
TNO

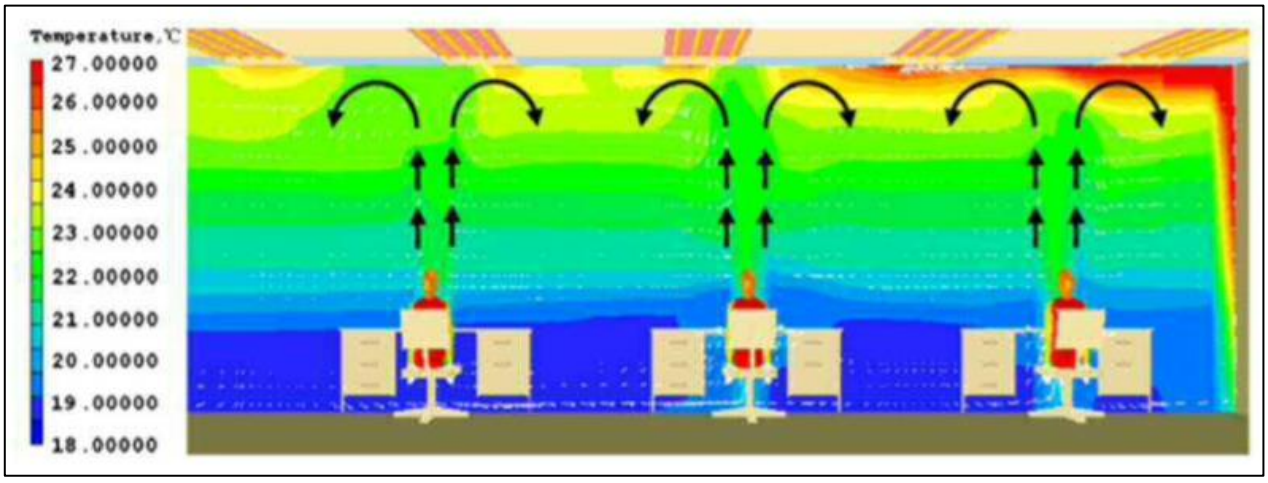
Temperature,℃
27.00000
26.00000
25.00000
24.00000
23.00000
22.00000
21.00000
20.00000
19.00000
18.00000

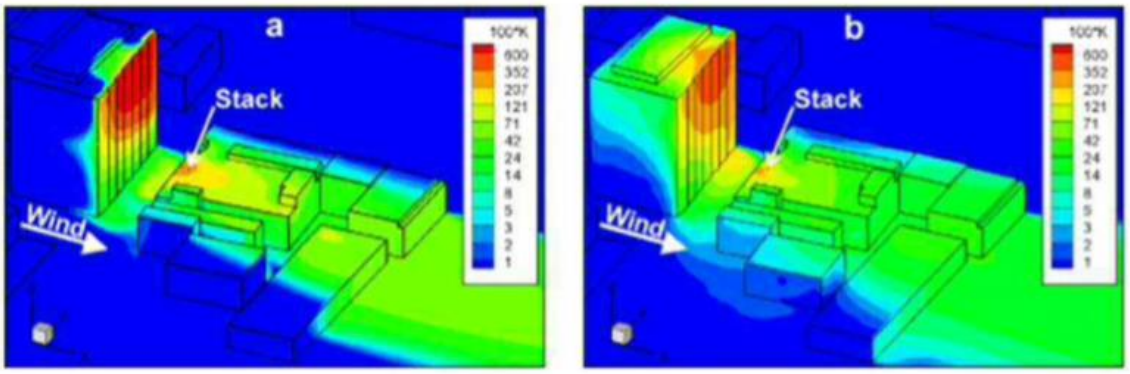
a
Stack
Wind
100°K
600
352
207
121
71
42
24
14
8
5
3
2
1
b
Stack
Wind
100°K
600
352
207
121
71
42
24
14
8
5
3
2
1

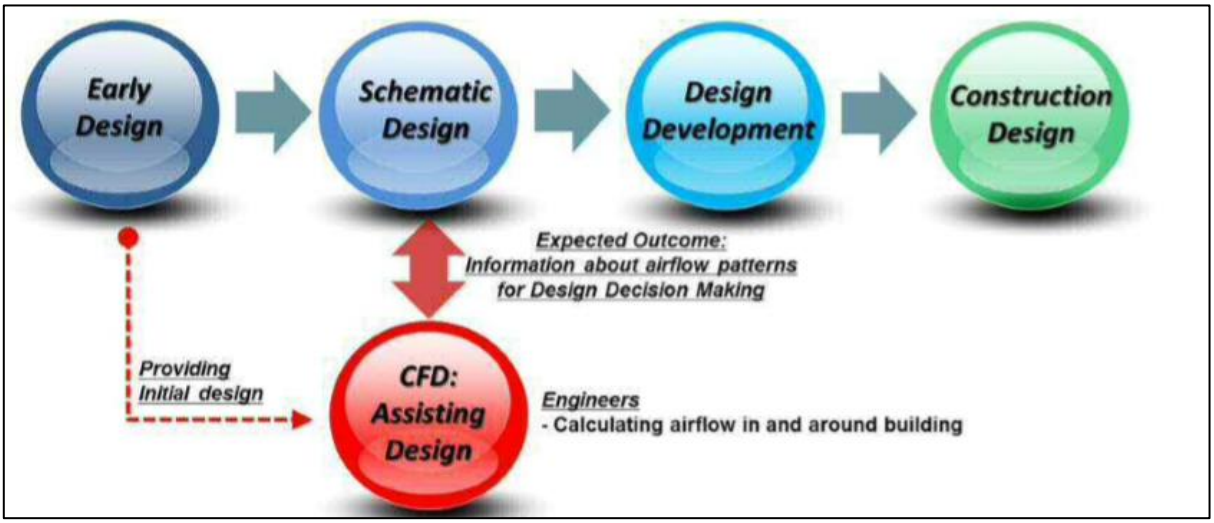
Early Design
Schematic Design
Design Development
Construction Design
Expected Outcome:
Information about airflow patterns
for Design Decision Making
Providing
Initial design
CFD:
Assisting
Design
Engineers
- Calculating airflow in and around building

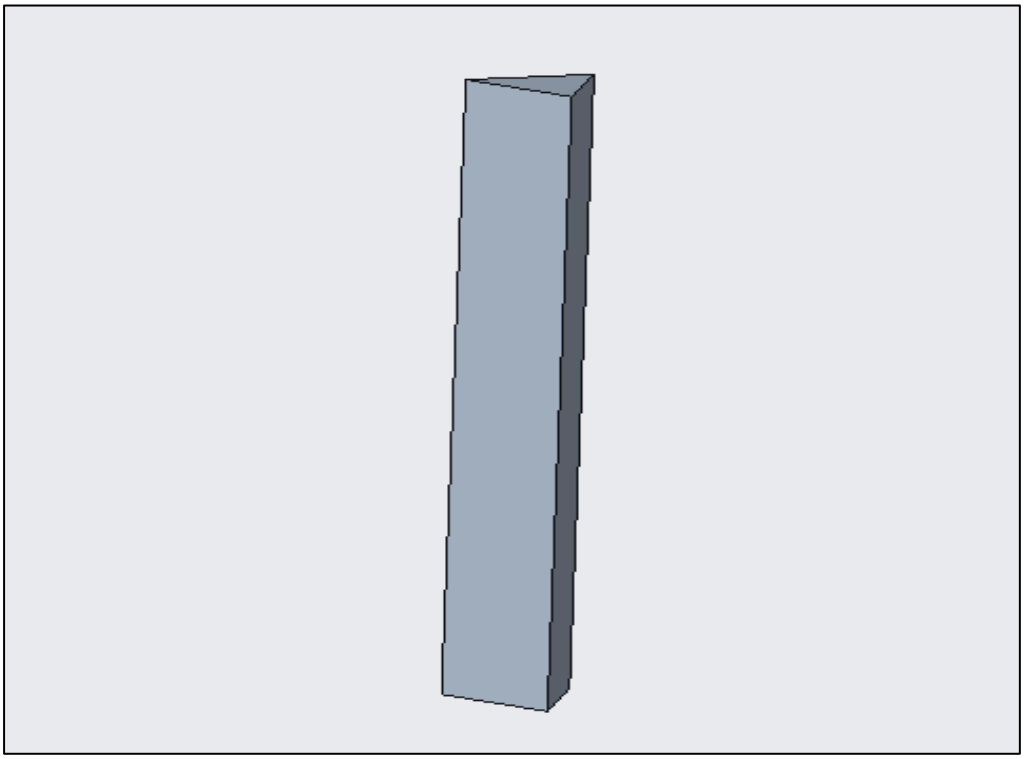

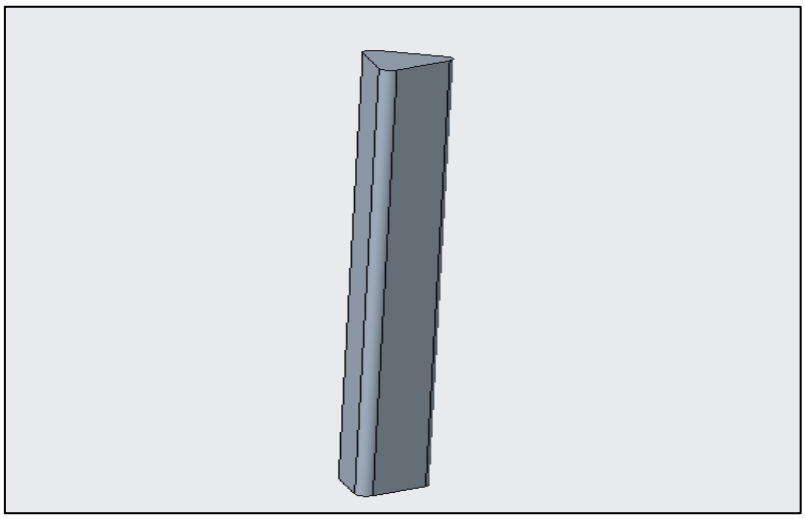

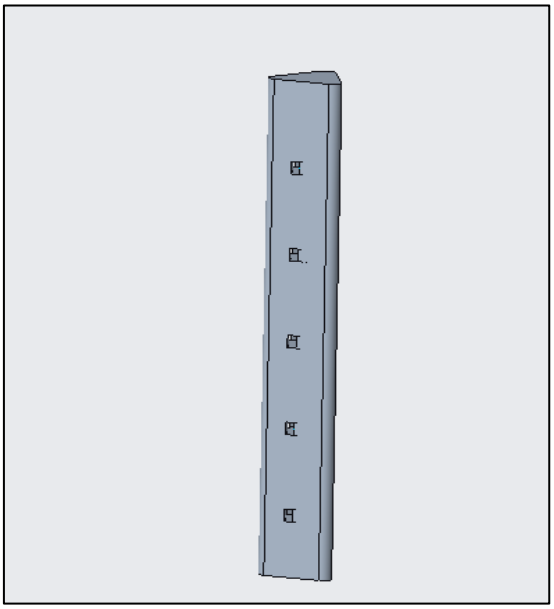

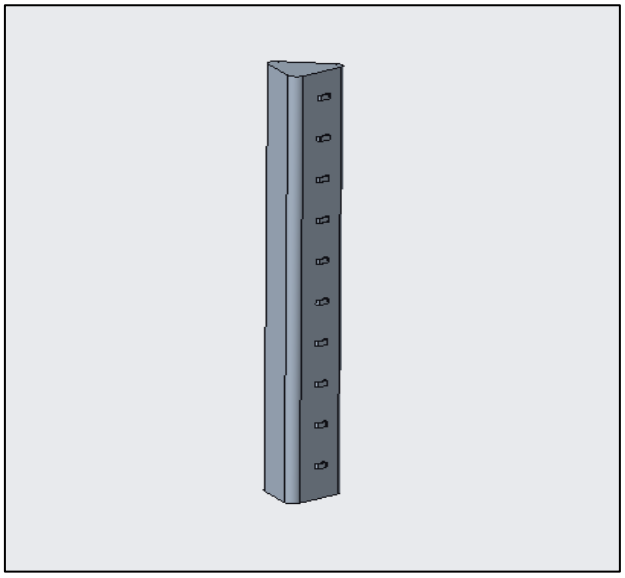

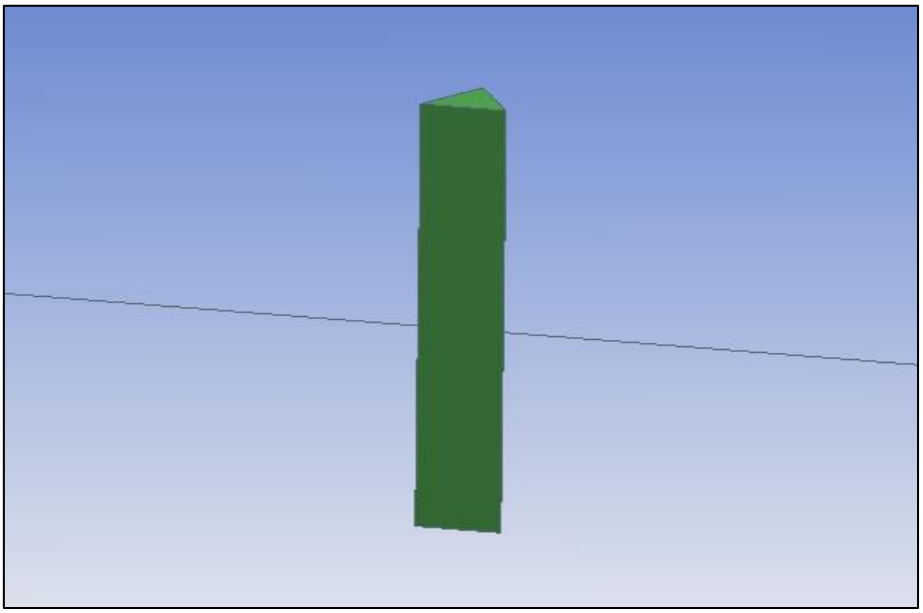

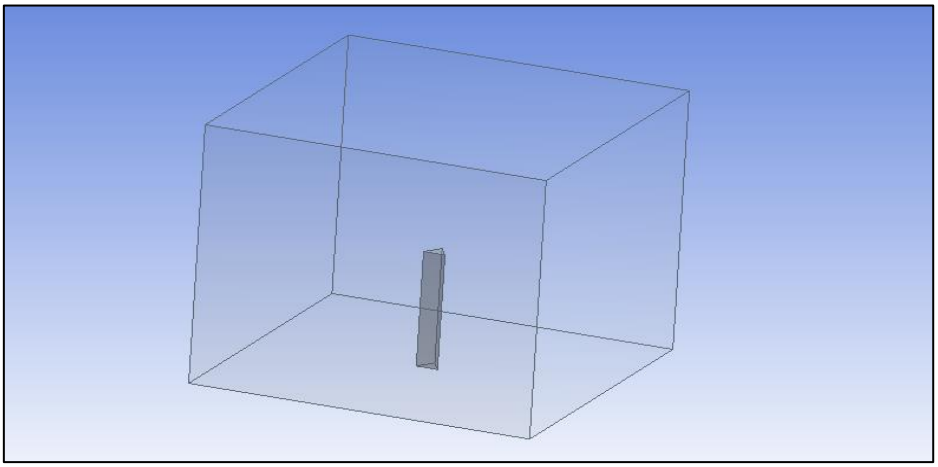

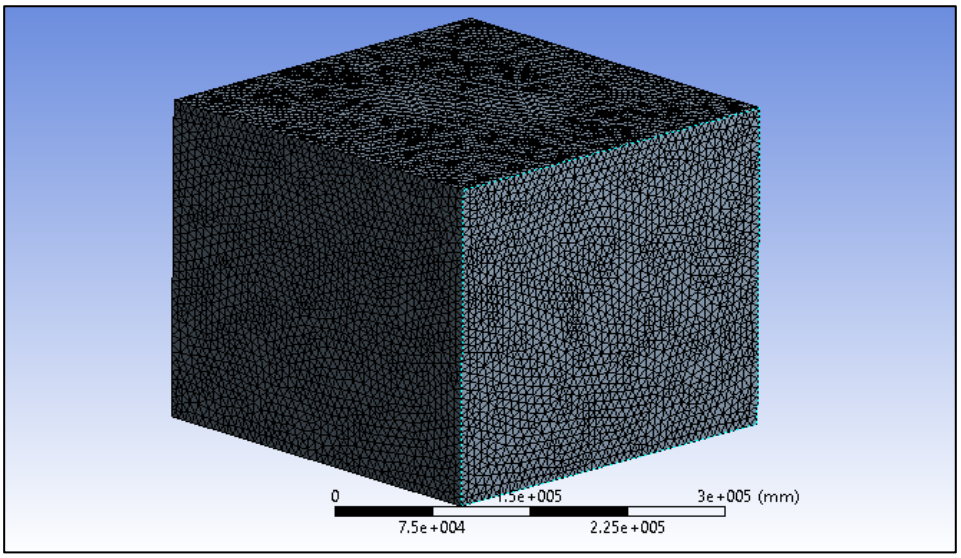
0
1.5e+005
3e+005 (mm)
7.5e+004
2.25e+005

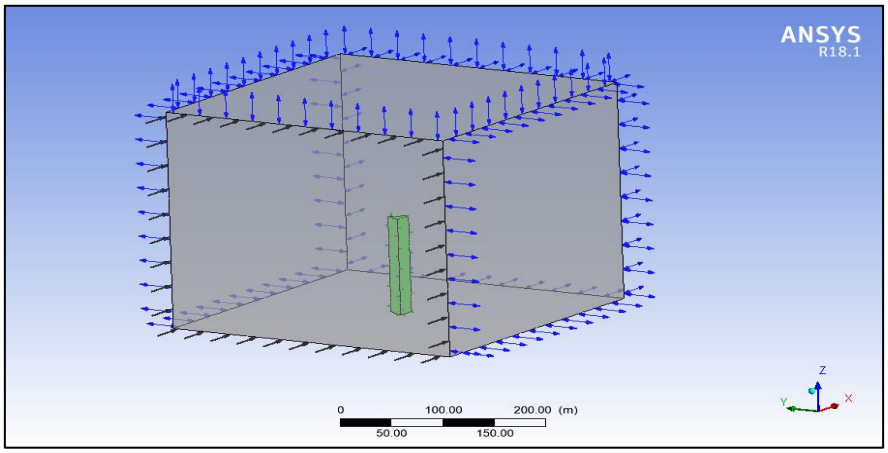
ANSYS
R18.1
0
100.00
200.00 (m)
50.00
150.00
Z
Y
X

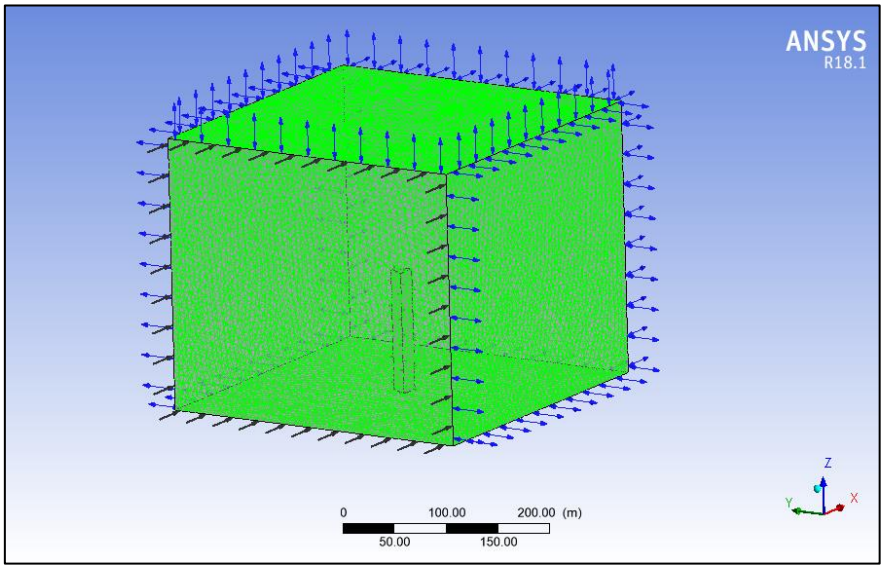
ANSYS
R18.1
0
100.00
200.00 (m)
50.00
150.00
Z
Y
X

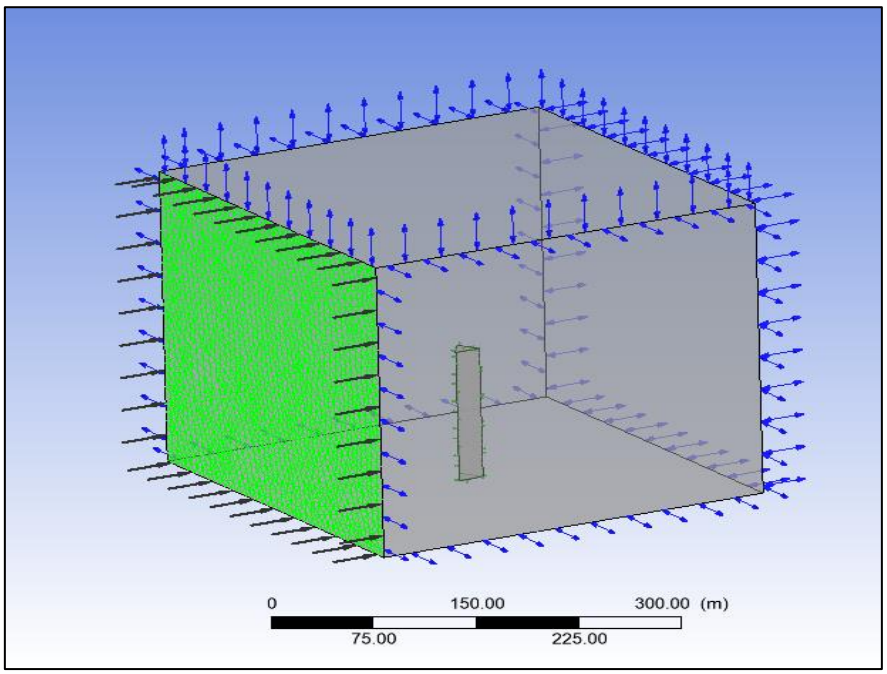
0
150.00
300.00 (m)
75.00
225.00

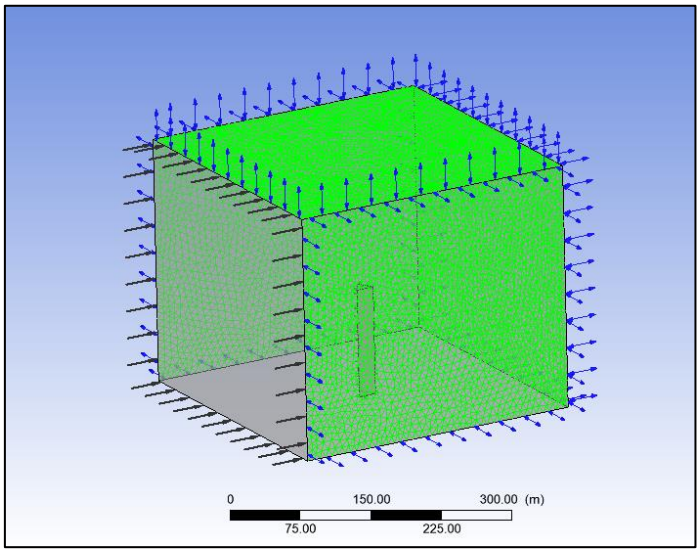
0
150.00
300.00 (m)
75.00
225.00

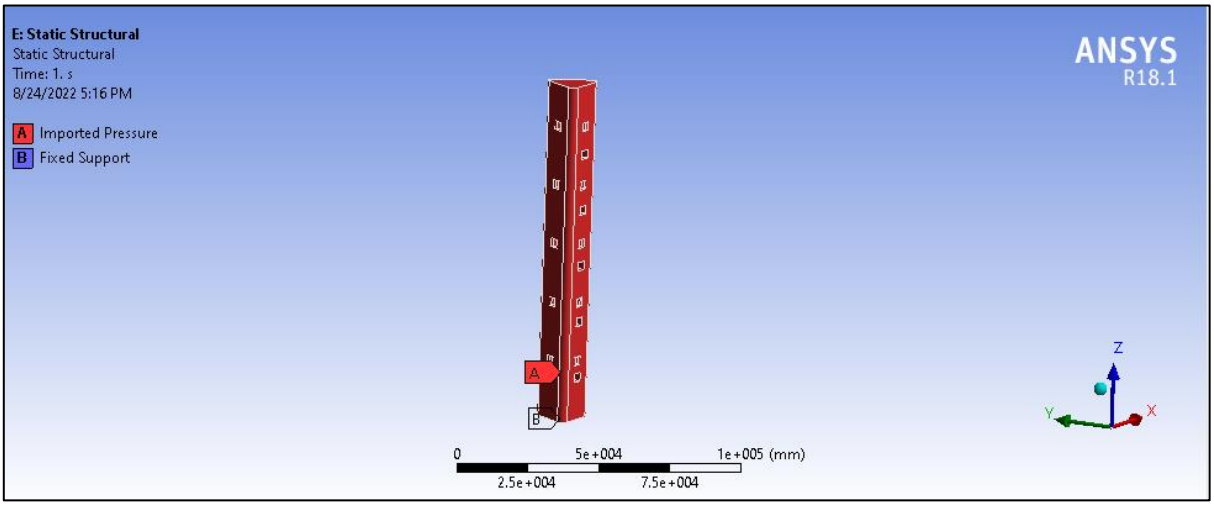
E: Static Structural
Static Structural
Time: 1. s
8/24/2022 5:16 PM
A Imported Pressure
B Fixed Support
ANSYS
R18.1
Z
Y
X
0
5e+004
1e+005 (mm)
2.5e+004
7.5e+004

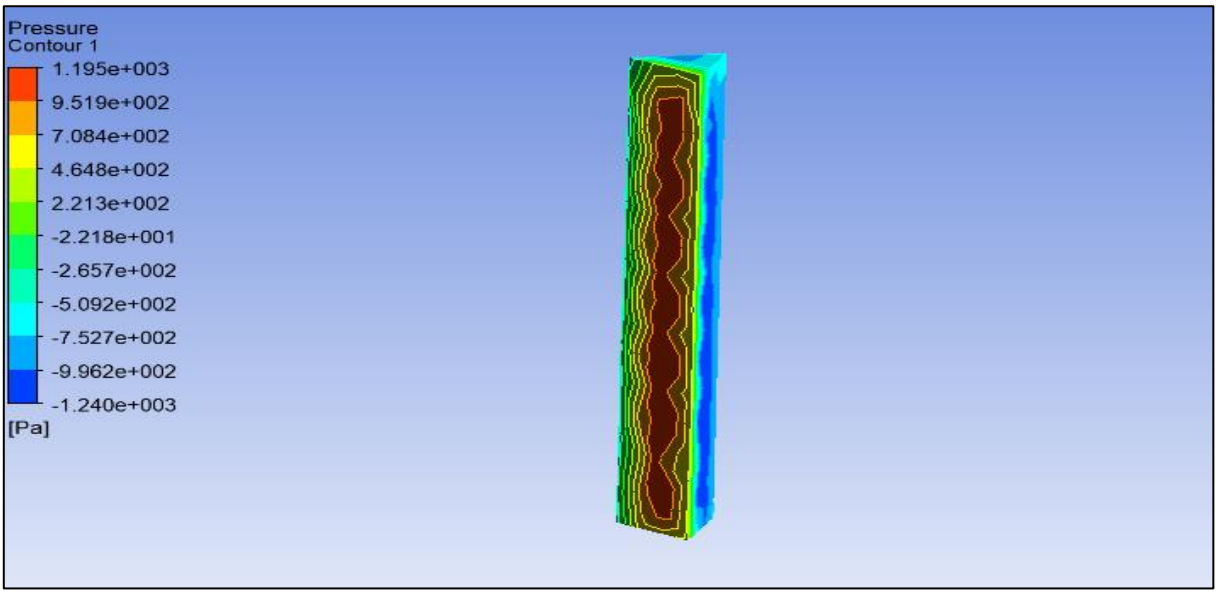
Pressure
Contour 1
1.195e+003
9.519e+002
7.084e+002
4.648e+002
2.213e+002
-2.218e+001
-2.657e+002
-5.092e+002
-7.527e+002
-9.962e+002
-1.240e+003
[Pa]

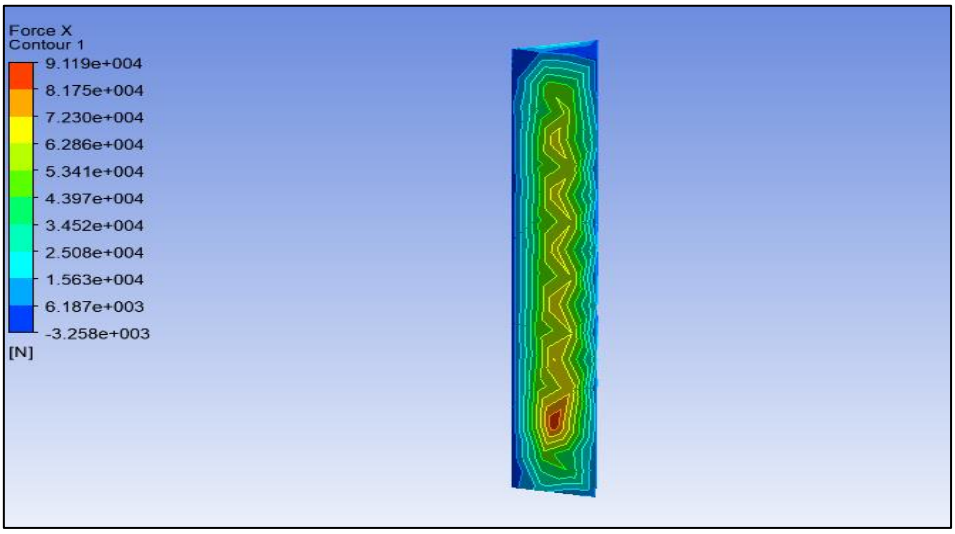
Force X
Contour 1
9.119e+004
8.175e+004
7.230e+004
6.286e+004
5.341e+004
4.397e+004
3.452e+004
2.508e+004
1.563e+004
6.187e+003
-3.258e+003
[N]

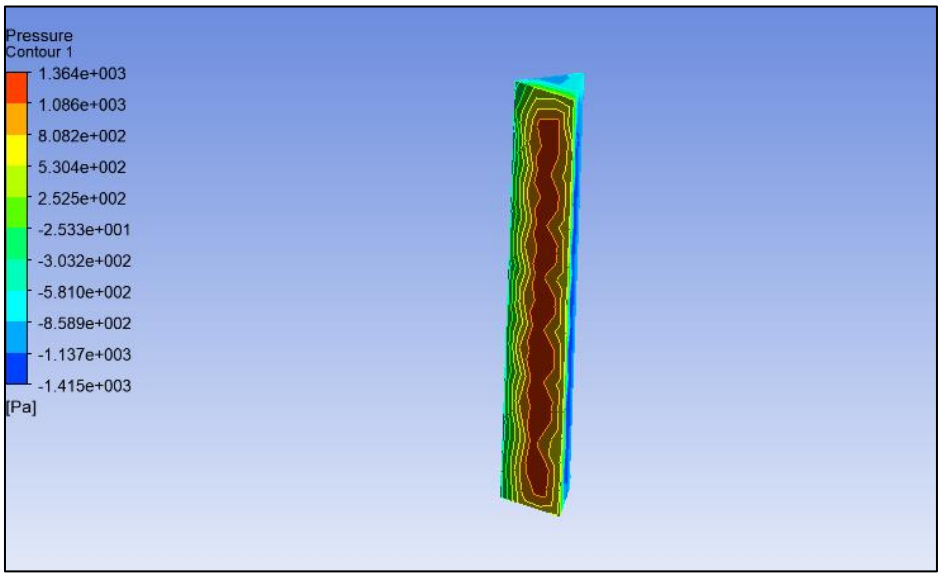
Pressure
Contour 1
1.364e+003
1.086e+003
8.082e+002
5.304e+002
2.525e+002
-2.533e+001
-3.032e+002
-5.810e+002
-8.589e+002
-1.137e+003
-1.415e+003
[Pa]

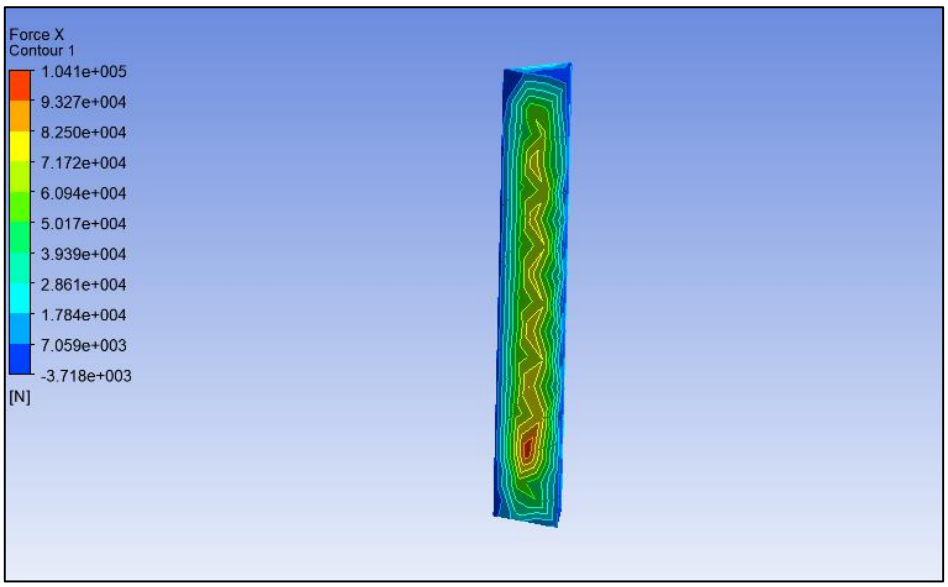
Force X
Contour 1
1.041e+005
9.327e+004
8.250e+004
7.172e+004
6.094e+004
5.017e+004
3.939e+004
2.861e+004
1.784e+004
7.059e+003
-3.718e+003
[N]

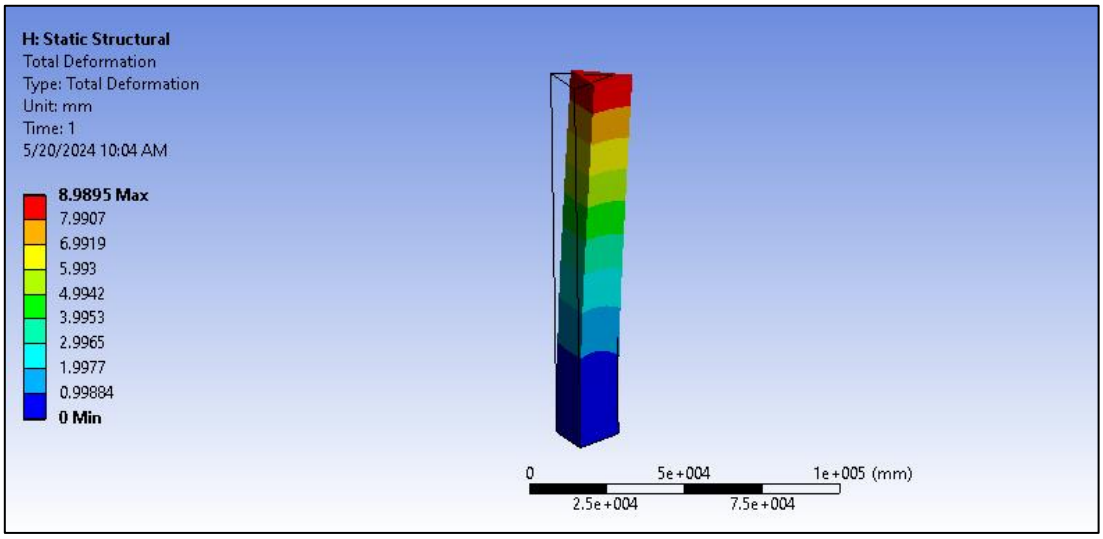
H: Static Structural
Total Deformation
Type: Total Deformation
Unit: mm
Time: 1
5/20/2024 10:04 AM
8.9895 Max
7.9907
6.9919
5.993
4.9942
3.9953
2.9965
1.9977
0.99884
0 Min
0
5e+004
1e+005 (mm)
2.5e+004
7.5e+004

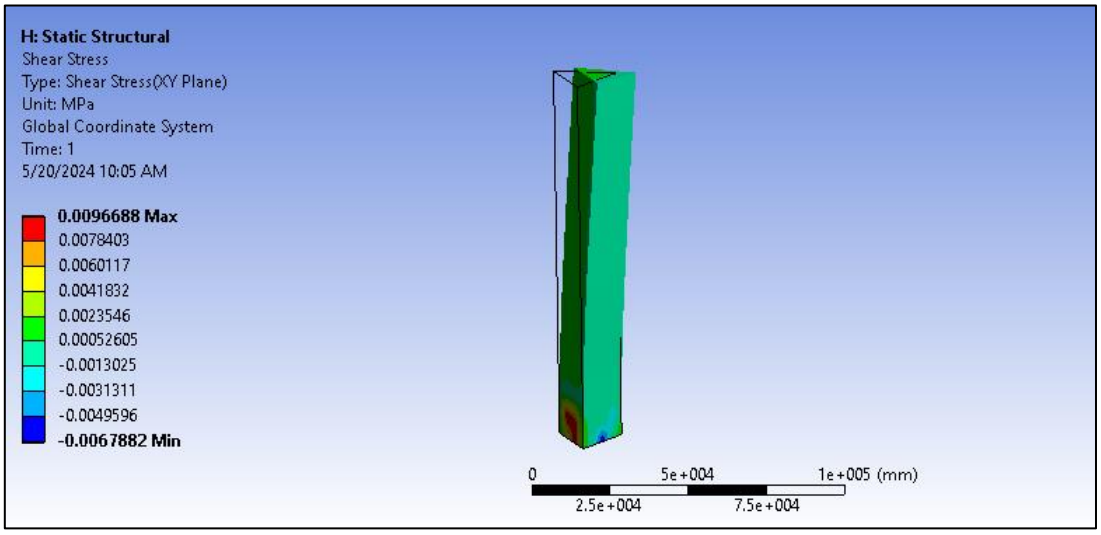
H: Static Structural
Shear Stress
Type: Shear Stress(XY Plane)
Unit: MPa
Global Coordinate System
Time: 1
5/20/2024 10:05 AM
0.0096688 Max
0.0078403
0.0060117
0.0041832
0.0023546
0.00052605
-0.0013025
-0.0031311
-0.0049596
-0.0067882 Min
0
5e+004
1e+005 (mm)
2.5e+004
7.5e+004

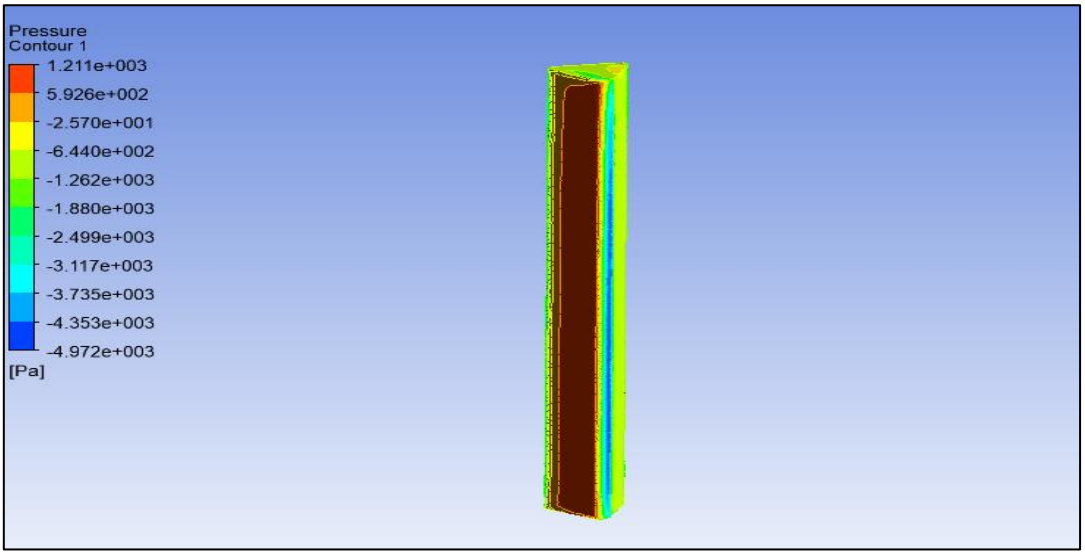
Pressure
Contour 1
1.211e+003
5.926e+002
-2.570e+001
-6.440e+002
-1.262e+003
-1.880e+003
-2.499e+003
-3.117e+003
-3.735e+003
-4.353e+003
-4.972e+003
[Pa]

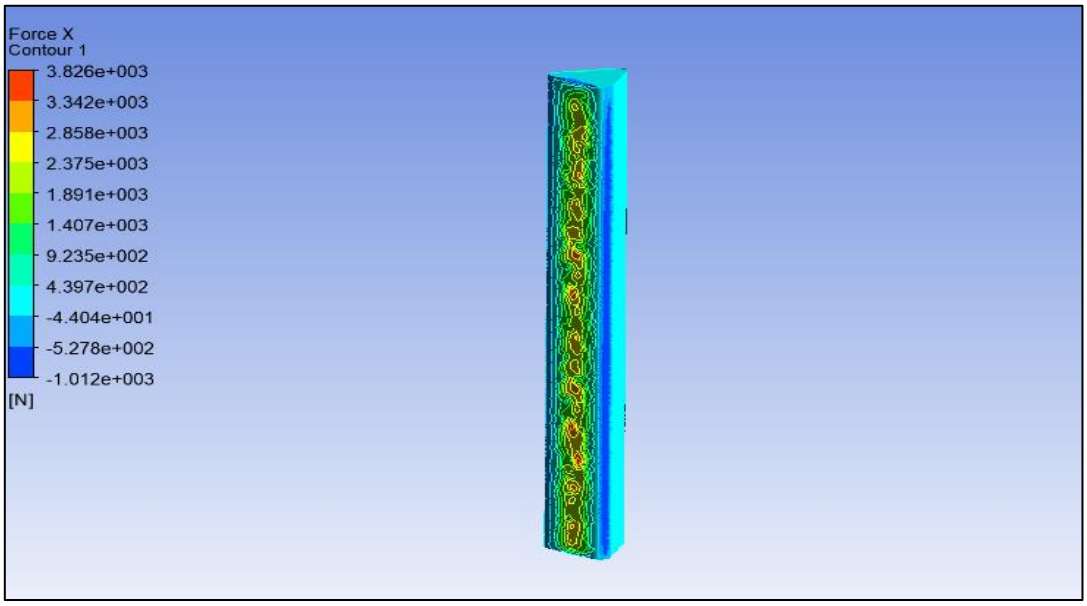
Force X
Contour 1
3.826e+003
3.342e+003
2.858e+003
2.375e+003
1.891e+003
1.407e+003
9.235e+002
4.397e+002
-4.404e+001
-5.278e+002
-1.012e+003
[N]

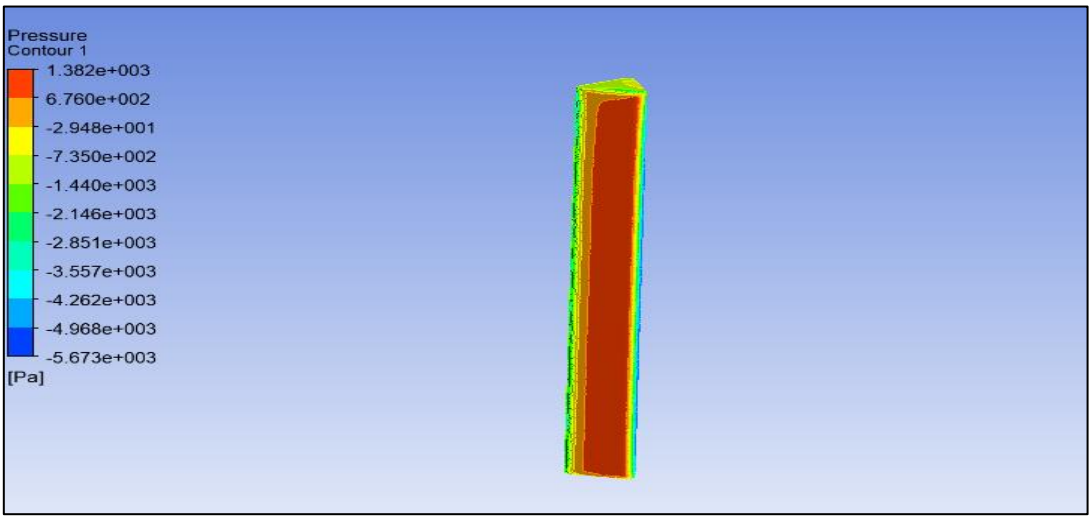
Pressure
Contour 1
1.382e+003
6.760e+002
-2.948e+001
-7.350e+002
-1.440e+003
-2.146e+003
-2.851e+003
-3.557e+003
-4.262e+003
-4.968e+003
-5.673e+003
[Pa]

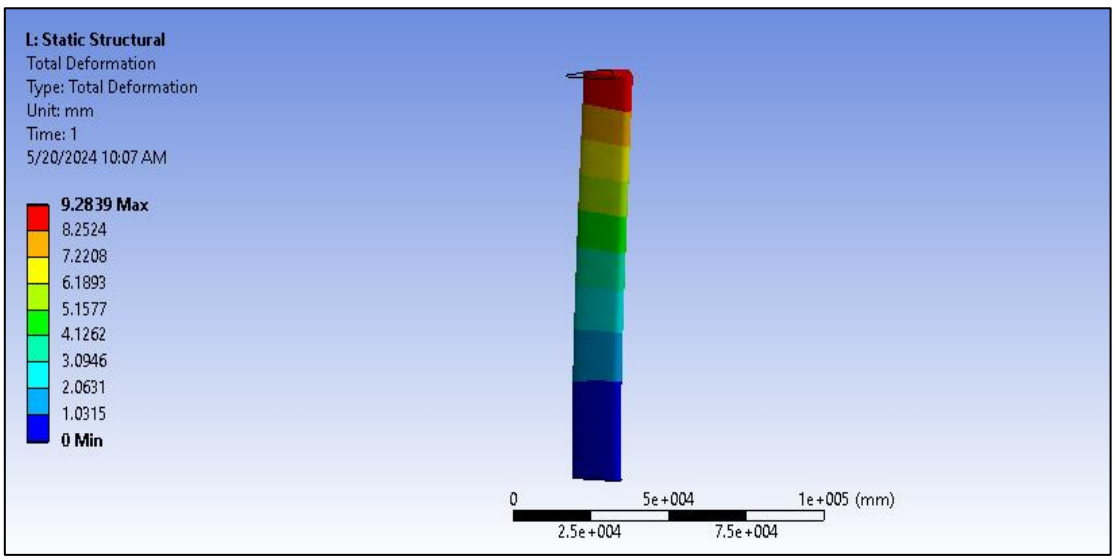
L: Static Structural
Total Deformation
Type: Total Deformation
Unit: mm
Time: 1
5/20/2024 10:07 AM
9.2839 Max
8.2524
7.2208
6.1893
5.1577
4.1262
3.0946
2.0631
1.0315
0 Min
0
5e+004
1e+005 (mm)
2.5e+004
7.5e+004

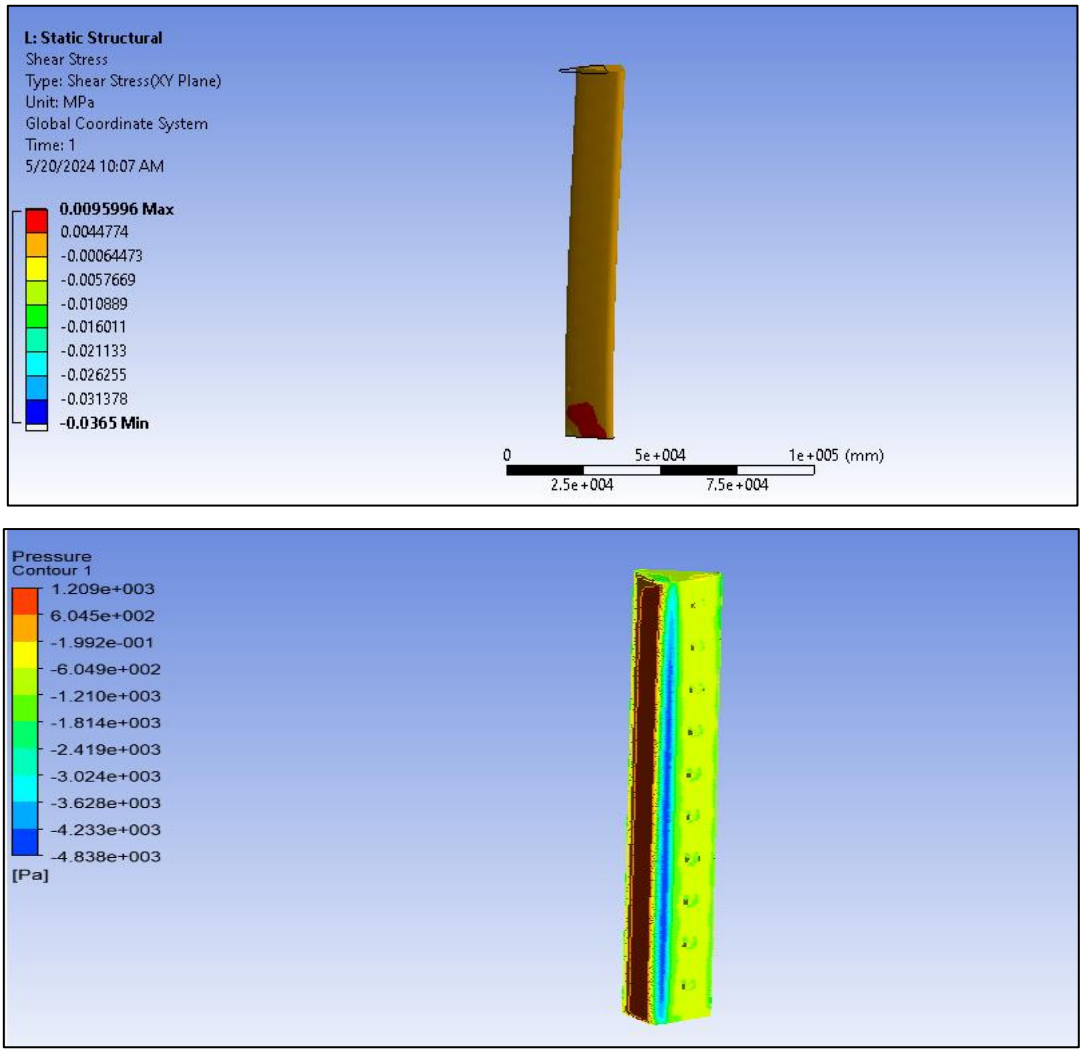

Tables

Table 5.1: Pressure Comparison for different designs

Design Type	Max Pressure@ 10m/s	Max Pressure@ 44m/s	Max Pressure@47 m/s
Triangular shape	61.77	1195	1364
Rounded Triangular Edge without opening	62.58	1211	1382
Rounded Triangular Edge with Balconies	62.5	1209	1380
Rounded Triangular Edge with Rounded Balconies	62.56	1210	1210
Rounded Triangular Edge with opening	62.85	1216	1388

Table 5.2: Fluid Structure Interaction (FSI) studies comparison

Design Type	Deformation (mm)	Shear stress (Mpa)
Triangular shape	8.9895	0.00966
Rounded Triangular Edge without opening	9.283	0.00959
Rounded Triangular Edge with Balconies	8.253	0.0293
Rounded Triangular Edge with Rounded Balconies	6.276	0.02193
Rounded Triangular Edge with opening	6.362	0.0153

Table captions

Table 5.1: Pressure Comparison for different designs

Table 5.2: Fluid Structure Interaction (FSI) studies comparison

.